ARTICLE

Channels and Transporters in Immunity

ORAI3 is dispensable for store-operated Ca²⁺ entry and immune responses by lymphocytes and macrophages

Liwei Wang[1]*, Lucile Noyer[1]* , Yin-Hu Wang[1]* , Anthony Y. Tao[1]*, Wenyi Li[1]* , Jingjie Zhu[1], Pedro Saavedra[1], Syed T. Hoda[1] , Jun Yang[1], and Stefan Feske[1]

Ca²⁺ signals regulate the function of many immune cells and promote immune responses to infection, cancer, and autoantigens. Ca²⁺ influx in immune cells is mediated by store-operated Ca²⁺ entry (SOCE) that results from the opening of Ca²⁺ release-activated Ca²⁺ (CRAC) channels. The CRAC channel is formed by three plasma membrane proteins, ORAI1, ORAI2, and ORAI3. Of these, ORAI1 is the best studied and plays important roles in immune function. By contrast, the physiological role of ORAI3 in immune cells remains elusive. We show here that ORAI3 is expressed in many immune cells including macrophages, B cells, and T cells. To investigate ORAI3 function in immune cells, we generated *Orai3⁻/⁻* mice. The development of lymphoid and myeloid cells in the thymus and bone marrow was normal in *Orai3⁻/⁻* mice, as was the composition of immune cells in secondary lymphoid organs. Deletion of *Orai3* did not affect SOCE in B cells and T cells but moderately enhanced SOCE in macrophages. *Orai3*-deficient macrophages, B cells, and T cells had normal effector functions in vitro. Immune responses in vivo, including humoral immunity (T cell dependent or independent) and antitumor immunity, were normal in *Orai3⁻/⁻* mice. Moreover, *Orai3⁻/⁻* mice showed no differences in susceptibility to septic shock, experimental autoimmune encephalomyelitis, or collagen-induced arthritis. We conclude that despite its expression in myeloid and lymphoid cells, ORAI3 appears to be dispensable or redundant for physiological and pathological immune responses mediated by these cells.

Introduction

Ca²⁺ is a universal second messenger that regulates the function of practically every cell type, including immune cells (Trebak and Kinet, 2019; Vaeth et al., 2020; Luan and Wang, 2021). Ca²⁺ signaling is mediated by the opening of Ca²⁺ channels in intracellular Ca²⁺ stores such as the ER and in the plasma membrane. Ca²⁺ release–activated Ca²⁺ (CRAC) channels play an important role in Ca²⁺ influx in immune cells, many other electrically nonexcitable cell types, skeletal muscle, and certain neurons (Prakriya and Lewis, 2015; Trebak and Kinet, 2019; Vaeth et al., 2020). The CRAC channel is formed by a small family of tetra-spanning membrane proteins called ORAI1, ORAI2, and ORAI3 (Prakriya and Lewis, 2015). Opening of the CRAC channel triggers store-operated Ca²⁺ entry (SOCE) across the plasma membrane. SOCE derives its name from the fact that its activation is

dependent on reduction of the Ca²⁺ concentration in ER stores. The release of Ca²⁺ from ER stores is mediated by the binding of the second messenger inositol 1,4,5-trisphosphate (IP₃) to Ca²⁺-permeable IP₃ receptor (IP₃R) channels and their subsequent opening. The resulting reduction in the ER Ca²⁺ concentration ([Ca²⁺]ᵢ) causes the dissociation of Ca²⁺ from two single-pass transmembrane proteins located in the ER membrane, stromal interaction molecule 1 (STIM1) and STIM2. Following Ca²⁺ dissociation from EF hands in STIM1 and STIM2, both proteins undergo conformational changes, which allow them to bind to and activate ORAI channels and induce SOCE (Prakriya and Lewis, 2015). All ORAI and STIM homologues were reported to participate in SOCE through CRAC channels in a variety of cell types (Emrich et al., 2021).

ORAI1 is the best-characterized ORAI family member. Its overexpression, together with STIM1, results in large Ca^{2+} currents that have most of the biophysical properties of native CRAC channels. The importance of ORAI1 for CRAC channel function and SOCE is highlighted by patients with loss-of-function mutations in the *ORAI1* gene that result in a genetic syndrome called CRAC channelopathy (Feske et al., 2006; Feske, 2010; Lacruz and Feske, 2015; Vaeth and Feske, 2018; Feske, 2019). These patients suffer from immunodeficiency with severe, recurrent infections, autoimmunity, muscular hypotonia, and ectodermal dysplasia (Feske, 2010; Lacruz and Feske, 2015). Genetic deletion of *Orai1* and *Stim1* genes in mice and other model organisms as well as pharmacological studies using CRAC channel inhibitors have identified many physiological functions of ORAI1, STIM1, and SOCE in a wide range of tissues and cell types (Feske, 2019; Bakowski et al., 2021). By contrast, the physiological roles of ORAI2 and ORAI3 are less well understood (Shuttleworth, 2012; Hoth and Niemeyer, 2013; Sanchez-Collado et al., 2021). We and others showed that ORAI2 contributes to SOCE in T cells, mast cells, and neutrophils and thereby regulates immune responses (Vaeth et al., 2017a; Tsvilovskyy et al., 2018; Grimes et al., 2020). In the central nervous system (CNS), ORAI2 appears to mediate the refilling of Ca^{2+} stores in hippocampal neurons (Chen-Engerer et al., 2019) and to promote neuronal death following ischemic stroke (Stegner et al., 2019).

Whereas ORAI1 and ORAI2 are present in all vertebrates, ORAI3 appears only in mammals and has likely evolved from ORAI1 (Cai, 2007; Shuttleworth, 2012). Whereas the protein sequence of its TM domains is highly conserved compared with ORAI1 and ORAI2, it is structurally distinct from the other two ORAIs, for instance because of a larger second extracellular loop between TM3 and TM4. When ectopically expressed, ORAI3 generates CRAC currents that are activated by store depletion, are Ca^{2+} selective, and show other characteristic features of native I_{CRAC} (DeHaven et al., 2007; Lis et al., 2007). In addition, ORAI3 currents have some unique features that distinguish them from ORAI1 and ORAI2, including a more pronounced fast Ca^{2+}-dependent inactivation and a STIM1-independent activation by the CRAC channel modulatory drug 2-aminoethoxydiphenyl borate (2-APB; Lis et al., 2007; Peinelt et al., 2008; Schindl et al., 2008; Zhang et al., 2008). Besides being involved in the formation of store-operated CRAC channels, ORAI3 has also been reported to form, together with ORAI1, the arachidonate acid (AA)–regulated Ca^{2+} (ARC) channel. This channel has biophysical properties similar to the CRAC channel, and its activation is dependent on STIM1. In contrast to CRAC channels, ARC channel activation is independent of store depletion and mediated instead by AA (Shuttleworth et al., 2004; Hoth and Niemeyer, 2013). The physiological and pathological significance of ARC channels remains unclear.

Several studies have suggested a role for ORAI3 in various types of cancers including breast, lung, prostate, and colorectal cancer, where it mediates SOCE as well as store-independent Ca^{2+} influx (Tanwar et al., 2020; Sanchez-Collado et al., 2021). Besides evidence from cancer cell lines, increased ORAI3 expression was reportedly associated with reduced survival of patients with lung adenocarcinoma and colorectal cancer

(Benzerdjeb et al., 2016; Ibrahim et al., 2019). ORAI3 mRNA is ubiquitously expressed in many organs and cell types in mice and humans. A recent study using mice with inducible, cardiomyocyte-specific deletion of *Orai3* revealed a function for ORAI3 in Ca^{2+} signaling in the heart and the prevention of dilated cardiomyopathy (Gammons et al., 2021). ORAI3 is also expressed in cells of the immune system (Vaeth et al., 2020), suggesting that it may contribute to Ca^{2+} influx and immune cell function. Stimulation of naive human T cells was reported to result in an increase in ORAI3 mRNA levels and the ratio of ORAI3 to ORAI1. Enhanced ORAI3 expression was associated with a reduced redox sensitivity of T cells because ORAI3, unlike ORAI1, lacks a cysteine residue that mediates suppression of CRAC channel function in response to H_2O_2 (Bogeski et al., 2010). Moreover, two recent studies implicated ORAI3 in the pathophysiology of rheumatoid arthritis (RA). $CD4^+$ T cells from RA patients had increased expression of ORAI3 (Ye et al., 2021). Deletion of ORAI3 in human T cells reduced AA-activated Ca^{2+} influx and impaired the ability of T cells to induce synovitis in a murine synovium model of RA. In another study, systemic silencing of ORAI3 expression by RNA interference attenuated collagen-induced arthritis (CIA) in mice (Liu et al., 2015). Whether ORAI3 promotes inflammation in other autoimmune diseases or physiological immune responses in vivo remains unknown.

We here show that ORAI3 is the most highly expressed ORAI paralog in many immune cell subsets, including B cells and macrophages. To study the significance of ORAI3 for immune cell function and immunity in vivo, we generated $Orai3^{-/-}$ mice. *Orai3* deficiency had no effects on the numbers and phenotype of lymphoid and myeloid cells in primary or secondary lymphoid organs. Deletion of *Orai3* did not affect SOCE in T and B cells following antigen-receptor stimulation, but moderately enhanced SOCE in macrophages, potentially indicating an inhibitory role of ORAI3 in CRAC channel regulation. Despite its robust expression in lymphoid and myeloid cells, the deletion of *Orai3* did not impair their function in vitro. Moreover, immune responses in vivo that depend on myeloid and lymphoid cell function were unaffected by the lack of *Orai3* expression, including T cell–dependent and –independent humoral immunity, sepsis, experimental autoimmune encephalomyelitis (EAE), CIA, and antitumor immunity. These results indicate that ORAI3 is dispensable, or at least redundant, for immune cell function and immune responses.

Materials and methods

Generation of $Orai3^{-/-}$ mice

$Orai3^{-/-}$ mice were generated using CRISPR-Cas9 genome editing. Briefly, two pairs of sgRNAs were designed to target exon 1 of the mouse *Orai3* gene (Table S1). sgRNAs were designed using the CRISPRtool (http://crispr.mit.edu) and Benchling sgRNA Designer (https://www.benchling.com/crispr/). Guide sequences were chosen by minimizing potential off-target effects (Ran et al., 2013) and maximizing on-target potential (Chari et al., 2015). sgRNAs were cloned into the pSIN sgRNA expression vector (Ng et al., 2019) and transcribed in vitro using the T7

transcription kit. Briefly, the T7 promoter was added to sgRNA sequences by PCR amplification using primers T7-sgRNA-F1 and T7-sgRNA-R (Table S1). The T7-sgRNA PCR product was gel purified and used as the template for in vitro transcription using the MEGAshortscript T7 kit (Life Technologies). sgRNAs were purified using the MEGAclear kit (Life Technologies), eluted in RNase-free water, and used for microinjection of zygotes from C57BL/6 mice together with recombinant Cas9 protein (kindly provided by James Muller, New York University, New York, NY). Cas9 protein (20 ng/μl) and sgRNAs (50 ng/μl) were mixed and injected into zygotes at the pronuclei stage, which were implanted into pseudo-pregnant female mice. Litters were genotyped by PCR amplification of *Orai3* exon 1 from tail DNA, cloning of PCR products into the pGEM-T vector, and sequencing of individual clones. We identified two strains of mice with nucleotide deletions in *Orai3* exon 1: Δ 17, in which nt 69–85 of the *Orai3* coding sequence were deleted (*Orai3*$^{\Delta 17}$), and Δ 85, in which nt 33–117 of the *Orai3* coding sequence were deleted (*Orai3*$^{\Delta 85}$). The Δ 17 and Δ 85 deletions were both predicted to result in a frameshift and premature termination of ORAI3 protein translation.

Genotyping of mice

WT, *Orai3*$^{\Delta 17}$, and *Orai3*$^{\Delta 85}$ mice were genotyped by PCR using oligonucleotide primers flanking the sgRNA target site: Orai3-F (37F), 5′-GTCCGTAACTGTTCCCGCTG-3′, and Orai3-R (394R), 5′-AGCCCGACAGCAGAGCAGATG-3′, yielding predicted amplicon sizes of 358 bp (WT) and 273 bp (*Orai3*$^{\Delta 85}$). PCR conditions for all reactions were as follows: denaturation at 95°C for 5 min, followed by 40 cycles of denaturation at 95°C for 30 s, annealing at 60°C for 30 s, and elongation at 72°C for 30 s, with an additional 10-min final elongation step at 72°C. Mice were maintained under specific pathogen-free conditions. All animal experiments were approved by the Institutional Animal Care and Use Committee at New York University Grossman School of Medicine.

Expression analysis

ImmGen and Haemopedia count files were downloaded from https://www.immgen.org (Heng et al., 2008) and https://www.haemosphere.org (de Graaf et al., 2016), respectively. Count values were normalized by the transcripts per million (TPM) method. Analyses and figures were generated using Matlab v2018 (MathWorks).

ORAI3 antibody staining

ORAI3 staining was performed in transfected Plat-E cells (Morita et al., 2000), bone marrow–derived macrophages (BMDMs), and B cells. Plat-E cells were transfected with pHAGE-msOrai3-IRES-GFP plasmid using GenJet (cat. no. SL100489; SignaGen Laboratories) following the manufacturer's instructions. 48 h after transfection, Plat-E cells were harvested by trypsinization, fixed with 4% PFA in PBS (cat. no. J19943-K2; Thermo Fisher Scientific) for 15 min, and permeabilized with permeabilization buffer (cat. no. 00-8333-56, Thermo Fisher Scientific) for 20 min. Cells were incubated for 20 min with a custom-made affinity-purified polyclonal rabbit anti-ORAI3

antibody that recognizes the last 17 amino acids at the C terminus of mouse ORAI3 protein: KQELEELSRLQGELQAV (1:500; Yen-Zym Antibodies). Cells were washed three times with PBS and stained with goat anti-rabbit IgG conjugated with Alexa Fluor 647 (1:2,000, cat. no. A32733; Thermo Fisher Scientific) for 15 min. ORAI3 staining of BMDMs and B cells was performed using the same protocol except plasmid transfection.

Immunization of mice and antibody detection by ELISA

Mice were injected i.p. with 100 μg NP-(27)-KLH (cat. no. N-5060-5-BS; BioCat) emulsified in Imject Alum (Thermo Fisher Scientific) or 50 μg NP50-AECM-Ficoll (cat. no. F-1420-10-BS; BioCat) plus 100 μg poly(I:C) (cat. no. P1530; Sigma-Aldrich) in PBS. Mouse sera were collected on days 7 and 14. For the detection of low-affinity (NP$_{25}$) or high-affinity (NP$_4$) antibodies in immunized mice, sera were tested in threefold serial dilutions starting from a 1:30 initial dilution. Antibody levels were measured using AP-conjugated goat anti-mouse IgM and IgG detection antibodies (1:2,000; cat. nos. 1021-04 and 1030-04; Southern Biotech). Phosphatase substrate kit was purchased from Sigma-Aldrich (cat. no. 37620). After addition of substrate solution, absorption was measured at 405 nm using a Flexstation 3 plate reader (Molecular Devices).

Retroviral transduction

Plat-E cells were transfected with retroviral expression plasmids encoding shRNAs targeting mouse *Orai3* (Table S1) and the ecotropic packaging vector pCL-Eco. Retroviral supernatant was collected 48 and 72 h after transfection and used to transduce primary mouse B cells 24 h after their stimulation with anti-RP105 (10 μg/ml). Retroviral transduction was conducted by spin infection (2,500 rpm) for 90 min at 32°C in the presence of 8 μg/ml polybrene (cat. no. 107689; Sigma-Aldrich).

T cell stimulation and differentiation

Total CD4$^+$ and CD8$^+$ T cells were isolated from mouse spleens using the MagniSort Mouse CD4 T cell Enrichment Kit (cat. no. 8804-6821-74; eBioscience) and MagniSort Mouse CD8 T cell Enrichment Kit (cat. no. 8804-6822-74; eBioscience), respectively. CD4$^+$ and CD8$^+$ T cells were stimulated with 1 μg/ml anti-CD3 (clone 2C11; BE0001-1; BioXCell) plus 1 μg/ml anti-CD28 antibodies (clone 37.51; BE0015-1; BioXCell) on plates coated with rabbit anti-hamster IgG (cat. no. MP0855398; MP Biomedicals). For differentiation of naive CD4$^+$ T cells into T helper 1 (Th1), Th17, and Th2 cells, T cells were polarized for 4 d with 20 ng/ml 1 IL-12 (cat. no. 210-12; PeproTech) and 5 mg/ml anti-IL-4 (cat. no. 12-7041-81; eBioscience) for Th1; 20 ng/ml IL-6 (cat. no. 406-ML-025; R&D Systems), 0.5 ng/ml TGFβ (cat. no. 100-21; PeproTech), 5 mg/ml anti-IL-4, and 5 mg/ml anti-IFNγ (clone XMG1.2; BioXcell) for Th17; 100 ng/ml IL-4 (cat. no. 214-14; PeproTech), 5 mg/ml anti–IL-12 (clone R1-5D9; BioXcell), and 5 mg/ml anti-IFNγ for Th2 cells in RPMI containing 2 mM L-glutamine, 50 mM 2-mercaptoethanol, 100 U/ml penicillin/ streptomycin, and 10% FCS. For differentiation of CD8$^+$ T cells into cytotoxic T lymphocytes (CTLs), T cell were detached 48 h after stimulation and resuspended in RPMI containing 100 IU/ml IL-2 for an additional 2 d. For cytokine expression, cells

were stimulated with 1 μM ionomycin (cat. no. 407952-1MG; Sigma-Aldrich) plus 20 nM PMA (cat. no. 524400; EMD Millipore) for 4 h in the presence of brefeldin A (cat. no. 00-4506-51; eBioscience) and analyzed by flow cytometry.

In vitro B cell assays

Splenic B cells were purified by negative selection using the Dynabeads Mouse CD43 kit (cat. no. 11422D; Invitrogen) and cultured in RPMI 1640 supplemented with 15% FBS, 2 mM L-glutamine, 99 μM 2-mercaptoethanol, 100 IU/ml penicillin/streptomycin, 1× nonessential amino acids, and 1 mM sodium pyruvate. Purified CD43$^-$ B cells were stimulated as indicated with 20 μg/ml LPS, 10 ng/ml recombinant murine IL-4 (cat. no. 214-14; PeproTech), 10 ng/ml IL-21 (cat. no. 210-21; PeproTech), 2 μg/ml anti-CD40 antibody (cat. no. 16-0409-81; Thermo Fisher Scientific), 100 ng/ml class B CpG (cat. no. tlrl-1826; InvivoGen), and/or 10 μg/ml F(ab')$_2$ anti-mouse IgM antibody (cat. no. 16-5092-85; Thermo Fisher Scientific). For measuring proliferation, purified B cells were stained with 2.5 μM CFSE prior to stimulation. Cells were collected at various time-points following stimulation and analyzed by flow cytometry.

T cell proliferation assay

1×10^6 splenocytes were loaded with CellTrace Violet (CTV; cat. no. C34557; Invitrogen) according to the manufacturer's instructions. Cells were stimulated with 1 μg/ml anti-CD3 (clone 2C11; BE0001-1; Bio X Cell) plus 1 μg/ml anti-CD28 antibodies (clone 37.51; BE0015-1; Bio X Cell) in plates coated with rabbit anti-hamster IgG (cat. no. MP0855398; MP Biomedicals) for 3 d. CTV dilution was monitored daily using an LSR Fortessa flow cytometer and FACSDiva Software (BD) and further analyzed with FlowJo Software (BD).

Differentiation and stimulation of BMDMs

Femurs and tibiae of mice were removed, and bone marrow was flushed out using a 0.45-mm-diameter needle and washed twice as described previously (Vaeth et al., 2015). Bone marrow cells were cultured in iMDM medium supplemented with 10% FBS, 100 IU/ml penicillin/streptomycin, and 20% L929 supernatant for 7 d, resulting in >95% CD11b$^+$ BMDMs. To induce polarization, BMDMs were stimulated for 16 h with either 100 ng/ml LPS-EB (cat. no. tlrl-eblps; InvivoGen) and 100 ng/ml interferon-γ (cat. no. 315-05; PeproTech) for M1 macrophage polarization, or 40 ng/ml recombinant murine IL-4 (cat. no. 214-14; PeproTech) and recombinant murine IL-13 (cat. no. 210-13; PeproTech) for M2 macrophage polarization. To induce a type I interferon response, BMDMs were transfected with 5 μg/ml poly(I:C) (cat. no. tlrl-pic; InvivoGen) or poly(dA:dT) (cat. no. P0883; Sigma-Aldrich) using GenJet and analyzed after 6 h. Alternatively, BMDMs were treated with 75 μg/ml DMXAA (cat. no. S1537; Selleckchem) for 2 h. To induce inflammasome activation, BMDMs were treated with 100 ng/ml LPS-EB (cat. no. tlrl-eblps; InvivoGen) for 4 h, followed by 5 μM ATP (cat. no. tlrl-atp; InvivoGen) for 45 min. For TLR and Dectin1 receptor stimulation, BMDMs were treated for 18 h with either 20 μg/ml Zymosan A from *Saccharomyces cerevisiae* (cat. no. Z4250; Sigma Aldrich), 1 μg/ml Imiquimod (cat. no. tlrl-imqs; InvivoGen), or 100 ng/ml LPS (InvivoGen).

Type I interferon production

1×10^6 total bone marrow cells were seeded in 96-well U bottom plates and stimulated with CpG-A (cat. no. Tlrl-2216-1; InvivoGen) for 24 h. Cell culture supernatants were harvested and IFNα protein levels were measured using a mouse IFNα ELISA (cat no. luex-mifnav2; InvivoGen).

Flow cytometry

Staining of cell surface or intracellular proteins with fluorescently labeled antibodies was carried out as described before (Vaeth et al., 2017b). Cytometric bead arrays (CBAs) were performed according to the manufacturer's manual (cat. no. 560485; BD). Briefly, serum samples were diluted in assay buffer at a 1:1 ratio followed by incubation with the capture beads mixture and PE-detect reagent for 2 h at room temperature. Samples were washed twice and resuspended in PBS. Samples were acquired using a LSR Fortessa flow cytometer (BD) and analyzed using FlowJo software (BD). A complete list of antibodies and their respective fluorescent conjugates can be found in Table S2.

Real-time PCR

Cells were lysed in TRIzol (cat. no. 10296010; Thermo Fisher Scientific) followed by chloroform addition and centrifugation to isolate mRNA in the aqueous phase. cDNA was synthesized using the iScript cDNA synthesis kit (cat. no. 170-8891; Bio-Rad). Real-time PCR was performed using the Maxima SYBR Green qPCR Master Mix (cat. no. K0221; Thermo Fisher Scientific). Transcript levels were normalized to the expression of housekeeping genes using the $2^{-\Delta CT}$ method. A complete list of primers used in this study can be found in Table S1.

Intracellular Ca^{2+} measurements

T cells and B cells were attached to translucent 96-well plates (cat. no. 353219; BD Falcon) coated with 0.01% poly-L-Lysine (cat. no. P8920; Sigma-Aldrich). B cells, T cells, and macrophages were loaded with 1 μM Fura-2-AM (cat. no. F1221; Invitrogen) and washed with Ca^{2+}-free Ringer solution (containing 155 mM NaCl, 4.5 mM KCl, 3 mM MgCl$_2$, 10 mM D-glucose, and 5 mM Na-Hepes, pH 7.4). Cells were kept in Ca^{2+}-free Ringer solution at the beginning of measurements followed by depletion of ER Ca^{2+} stores with 1 μM thapsigargin (TG; 586005; Sigma-Aldrich). Ringer solution containing 2 mM Ca^{2+} was added to cells (1 mM final extracellular Ca^{2+} concentration) to measure SOCE. B cell receptor (BCR)-induced Ca^{2+} signals were measured in Ca^{2+}-containing Ringer solution following stimulation with different concentrations of anti-mouse IgM antibody (cat. no. 115-095-020; Jackson ImmunoResearch). Fc receptor (FcR)-induced Ca^{2+} influx in macrophages was measured after incubation of cells with different concentrations of anti-CD16/32 (cat. no. BE0307; Bio X cell) for 30 min before recordings, followed by FcR crosslinking with 30 μg/ml goat anti-rat IgG antibody (clone Poly4054; cat. no. 405401; BioLegend). Alternatively, macrophages were kept in 2 mM Ca^{2+} Ringer solution and stimulated with 50 μM 2-APB (524-95-8; Tocris). To measure ARC channel activity, macrophages were stimulated with different concentrations of freshly prepared AA (A3611; 181198; Sigma Aldrich),

followed by addition of either 1 µM ionomycin or TG to activate CRAC channels. T cell receptor (TCR)-induced Ca^{2+} influx in T cells was measured following incubation of cells with 1 µg/ml anti-CD3ε (clone 2C11) for 30 min before recordings. Cells were washed and kept in Ca^{2+}-free Ringer solution at the beginning of the recording, followed by CD3 crosslinking with 1 µg/ml rabbit anti-hamster IgG (MP0855398; MP Biomedicals) and readdition of 1 mM Ca^{2+} Ringer solution. Ca^{2+} influx in splenocytes isolated from mice with CIA was measured after loading cells with 1 µM Indo-1-AM (cat. no. I1223; Invitrogen) and stimulation with 1 µM TG using an LSR Fortessa (BD) flow cytometer. Indo-1 fluorescence was measured after 355-nm excitation (UV laser) and collected at 396 nm (379/28 filter) and 496 nm (515/30 filter) and plotted as the F396/F496 ratio. Fura-2 fluorescence was measured using a Flexstation 3 plate reader (Molecular Devices) at an emission wavelength of 510 nm after excitation at 340 and 380 nm every 5 s and plotted as F340/F380 emission ratio. Alternatively, Fura-2 fluorescence was measured using an Olympus IX81 inverted epifluorescence microscope, an Olympus Fluor objective and DG-5 xenon lamp (Sutter instrument) light source. At least 10 individual cells were averaged per recording. Microscopy data were analyzed using NIH ImageJ Fiji and Matlab (MathWorks).

Septic shock model

The induction of septic shock was carried out as previously described (Kayagaki et al., 2015). Briefly, mice aged 8–12 wk were injected intraperitoneally with 54 mg/kg LPS (cat. no. L2630-25MG; Sigma-Aldrich) and monitored eight times daily for a total of 2 d. Animals were euthanized when they reached a score of 4 in any of the eight parameters using the M-CASS (mouse clinical assessment scoring system; Lilley et al., 2015). Statistical analysis was performed with the log-rank (Mantel–Cox) test using Prism. No randomization or blinding was used for the animal studies.

Tumor allografts

B16-ovalbumin (OVA) melanoma cells (kind gift from Dr. Hongbo Chi, St. Jude Children's Research Hospital, Memphis, TN) were grown in DMEM medium supplemented with 10% FCS and 100 IU/ml penicillin/streptomycin. 3×10^5 B16-OVA cells were s.c. injected into 8–12 wk old C57BL/6 mice. 9 d later, mice were irradiated sublethally (6 Gy). The following day, mice were injected i.v. with 3×10^6 CD8$^+$ T cells isolated from OT-I mice. Naive CD8$^+$ T cells had been isolated from the spleen and peripheral lymph nodes of OT-I mice or OT-I $Orai3^{-/-}$ mice using a naive CD8α$^+$ T cell isolation kit (cat. no. 8804-6822-74; Invitrogen). Purified CD8$^+$ T cells were stimulated in vitro with 1 µg/ml anti-CD3 (clone 2C11; BE0001-1; Bio X Cell) and 1 µg/ml anti-CD28 antibodies (clone 37.51; BE0015-1; Bio X Cell) in plates coated with rabbit anti-hamster IgG (cat no. MP0855398; MP Biomedicals) for 48 h. Cells were then cultured with human IL-2 (20 IU/ml; cat. no. 200-02; PeproTech), mouse IL-7 (2.5 ng/ml; cat. no. 217-17; PeproTech) and IL-15 (25 ng/ml; cat. no. 210-15; PeproTech) for an additional 4 d before injection. Tumor-bearing mice were injected either separately with OT-I mice or OT-I $Orai3^{-/-}$ CD8$^+$ T cells, or with a 1:1 mixture of WT and $Orai3$-deficient cells. Tumor size was assessed every other day using a caliper. For some experiments, tumor tissue was harvested digested with 1 mg/ml collagenase type I (cat. no. CLS-1 LS004196; Worthington) and 100 µg/ml DNase I (cat. no. 10104159001; Roche) and T cell infiltration analyzed by flow cytometry.

EAE

EAE was induced as previously described (Kaufmann et al., 2016). Briefly, mice were immunized s.c. with 200 µg myelin oligodendrocyte glycoprotein (MOG$_{35-55}$) peptide (cat. no. 60130-5; Anaspec) emulsified in incomplete Freund's adjuvant (IFA; cat. no. 263910; Difco) and heat-killed $Mycobacterium\ tuberculosis$ H37RA (cat. no. 231141; Difco). On days 0 and 2, mice were injected i.p. with 200 ng pertussis toxin (cat. no.180; List Biological Laboratories). Mice were evaluated for EAE symptoms every 2 d. The severity of EAE was analyzed according to the following clinical scoring system: 0 = no disease; 0.5 = partially limp tail; 1 = paralyzed tail; 2 = hind limb weakness; 3 = hind limb paralysis; 3.5 = hind limb paralysis and hunched back; 4 = hind and fore limb paralysis; 5 = moribundity and death (Kaufmann et al., 2016). All animals were provided with wet food on the floor. Mice were euthanized when they reached an EAE score of 4. At the end of the experiment, cells were isolated from the spinal cord (CNS) and spleen of mice and analyzed by flow cytometry.

CIA

CIA was induced as previously described (Inglis et al., 2008). Briefly, 10–14-wk-old mice were immunized intradermally at two sites near the root of the tail with 50 µl emulsion of 4 mg/ml chicken type II collagen (cat. no. C9301; Sigma-Aldrich) emulsified with an equal volume of IFA containing 10 mg/ml heated-killed $M.\ tuberculosis$ H37Rα (cat. no. 231141; Difco). A booster injection was administered on day 14 or 21 with the emulsion of collagen II and IFA (cat. no. 263910; Difco). The severity of arthritis was evaluated twice a week. Each paw was scored individually as follows: 0 = normal, 1 = slight swelling and/or erythema, 2 = pronounced swelling, and 3 = ankylosis (Tang et al., 2011). For the histological analysis of hind paws of mice, tissues were fixed in 4% PFA for 2 d, and bones were decalcified in 0.5 M EDTA for 28 d. Paraffin sections of paws were cut at 5 µm and stained with H&E. The evaluation of synovitis, pannus formation, and bone and cartilage destruction was conducted by a pathologist blinded to the experimental conditions, according to a graded scale as described previously (Tang et al., 2011).

ELISA

To analyze type II collagen antibodies in mice with CIA, 96-well plates were coated with 50 µl collagen II (10 µg/ml) overnight at 4°C, followed by blocking with 5% (w/v) BSA in PBS for 1 h at room temperature. Plates were incubated at room temperature for 2 h with serum isolated from mice with CIA, starting with a 1:90 dilution. AP-conjugated goat anti-mouse IgG (cat. no. 1030-0; SouthernBiotech) was added and incubated at room temperature for 1 h, followed by incubation with 50 µl/well substrate for 30 min in the dark at room temperature. The absorbance was measured at 405 nm using a FlexStation3 plate reader.

Statistical analysis

All results are shown as means with or without SEM. Data were analyzed with Prism 9 (GraphPad Software). The data distribution was assumed to be normal. The statistical significance of differences between experimental groups was determined by unpaired Student's *t* test unless stated otherwise or by paired Student's *t* test as indicated in the figure legends. Exact P values are indicated in the figures. The number of mice per experimental group is indicated in the figure legends.

Online supplemental material

Fig. S1 shows an expression analysis of *Orai3* in immune cells. Fig. S2 shows deletion of Orai3 in B cells and BMDMs without compensatory upregulation of *Orai1*, *Orai2* or *Stim1*, *Stim2* genes. Fig. S3 shows that B cells from *Orai3*$^{-/-}$ mice have normal SOCE. Fig. S4 shows that B cell development and immune responses to TI antigens are normal in *Orai3*$^{-/-}$ mice. Fig. S5 shows normal development of macrophages and dendritic cells (DCs) in *Orai3*$^{-/-}$ mice. Fig. S6 shows normal FcR-induced SOCE in *Orai3*-deficient macrophages and no evidence of AA-induced Ca^{2+} influx in WT BMDMs. Fig. S7 shows normal function of BMDMs and plasmacytoid DCs (pDCs) from *Orai3*$^{-/-}$ mice. Fig. S8 shows that *Orai3*$^{-/-}$ mice have normal T cell development. Fig. S9 shows that TG-induced SOCE is unimpaired in CD4$^+$ and CD8$^+$ T cells from *Orai3*$^{-/-}$ mice. Fig. S10 shows that *Orai3* deletion does not protect mice from induction of CIA. Table S1 provides the sequences of all sgRNAs, shRNAs, genomic PCR primers, and qRT-PCR primers used in this study. Table S2 provides a list of all antibodies used for flow cytometry in this study.

Results

ORAI3 is expressed in many immune cell types

To assess the role of ORAI3 in immune function, we analyzed *Orai3* mRNA expression in different murine immune cell subsets in relation to *Orai1* and *Orai2*, using the ImmGen and Haemopedia RNA-seq datasets. We reasoned that cells with high ORAI3 levels relative to ORAI1 or ORAI2 may be more dependent on ORAI3 for antigen receptor–induced Ca^{2+} influx and thus immune function. We observed that many murine immune cells have high relative *Orai3* expression compared with *Orai1* and *Orai2* (Figs. 1 A and S1 A). This is particularly true for B cell subsets including marginal zone and follicular B cells, plasma cells and plasma blasts, and to a lesser degree, macrophages. Other immune cells with high *Orai3* levels are mast cells and pDCs. By contrast, T lineage cells including CD4$^+$, CD8$^+$, and T regulatory (Treg) cells exhibit lower *Orai3* mRNA expression relative to *Orai1*. The levels of *Orai3* mRNA in different murine immune cell types correlated well between ImmGen and Haemopedia databases (Fig. S1 B). Collectively, these data indicate that *Orai3* is expressed in a variety of immune cells and may contribute to their function.

Genetic deletion of *Orai3* does not impair the development and viability of mice

To investigate the functional role of ORAI3 in immune cell function and immunity, we generated mice with germline deletion of *Orai3* by using CRISPR-Cas9 genome editing. Two sgRNAs, both targeting exon 1 of the *Orai3* gene locus, were used to inject zygotes of C57BL/6 mice and create an insertion-deletion (INDEL) mutation to abrogate *Orai3* expression (Fig. 1 B). Genotyping of mice detected several INDELs, two of which were chosen for further analysis. The Δ 17 strain (*Orai3*^{Δ17}) lacked nt 69–85 of the *Orai3* coding sequence, and the Δ 85 strain (*Orai3*^{Δ85}) lacked nt 33–117 (Fig. 1 C). Both deletions are predicted to result in a frameshift and premature termination of ORAI3 protein translation. Translation initiation of *Orai3* occurs at an ATG encoded by nt 175–177. Analysis of mouse *Orai3* mRNA predicted at least two potential alternative transcription initiation sites (TISs) at nt 289 and 400, which are both located 3′ of the Δ17 deletion and may therefore result in translation of an N-terminally truncated ORAI3 protein. The premise for this assumption is provided by the existence of a short, N-terminally truncated version of human ORAI1 (ORAI1β) whose translation is initiated at methionine 64 (Fukushima et al., 2012). To avoid expression of a putative short, N-terminally truncated ORAI3 isoform and thus incomplete deletion of ORAI3, we decided to use the *Orai3*^{Δ85} strain, in which the alternative TIS at nt 289 is deleted, for our studies. The TIS at nt 400 is still present in *Orai3*^{Δ85} mice, but would result in translation of an ORAI3 protein that lacks most of its first transmembrane domain, which encodes the pore of the CRAC channel, and would therefore likely result in a nonfunctional protein. To confirm deletion of ORAI3 protein expression in *Orai3*^{Δ85} mice, we used a custom-generated anti-ORAI3 antibody that recognizes an epitope in the C terminus of ORAI3. The antibody correctly detected an ORAI3-GFP fusion protein overexpressed in Plat-E cells (Fig. 1 D). We next used BMDMs cultured in vitro and B cells isolated from the spleen of mice to confirm ORAI3 protein deletion in homozygous *Orai3*^{Δ85} mice. ORAI3 antibody staining in BMDM from *Orai3*^{Δ85} mice was significantly reduced compared to WT mice (Fig. 1 E). A similar reduction was observed in B cells of *Orai3*^{Δ85} mice compared with WT controls (Fig. S2 A). To confirm that ORAI3 protein is indeed absent, we transduced B cells from WT and *Orai3*^{Δ85} mice with shRNA targeting *Orai3*. ORAI3 protein levels detected by flow cytometry were similar in WT B cells transduced with shOrai3 and B cells from *Orai3*^{Δ85} mice (Fig. S2 B). Moreover, shOrai3 transduction of *Orai3*^{Δ85} B cells did not result in further reduction of the ORAI3 protein signal. We conclude that ORAI3 is not expressed in *Orai3*^{Δ85} mice, which we refer to as *Orai3*$^{-/-}$ mice from here on out. To exclude potential compensatory effects resulting from the upregulation of other ORAI (and STIM) homologues in *Orai3*$^{-/-}$ mice, we measured the levels of *Orai1*, *Orai2*, *Stim1*, and *Stim2* mRNA in their macrophages and B cells but failed to observe any significant changes compared with WT mice (Fig. S2, C and D). ORAI3 is distinguished from its homologues ORAI1 and ORAI2 in that it can be directly gated by 2-APB when overexpressed in cell lines. Whether this is true for endogenously expressed ORAI3, which is likely to form heteromeric channel complexes with other ORAI homologues, is unknown. To investigate if endogenous ORAI3 is responsive to 2-APB and whether this response is impaired in *Orai3*$^{-/-}$ mice, we stimulated BMDMs from WT and *Orai3*$^{-/-}$ mice with 50 µM 2-APB in the presence
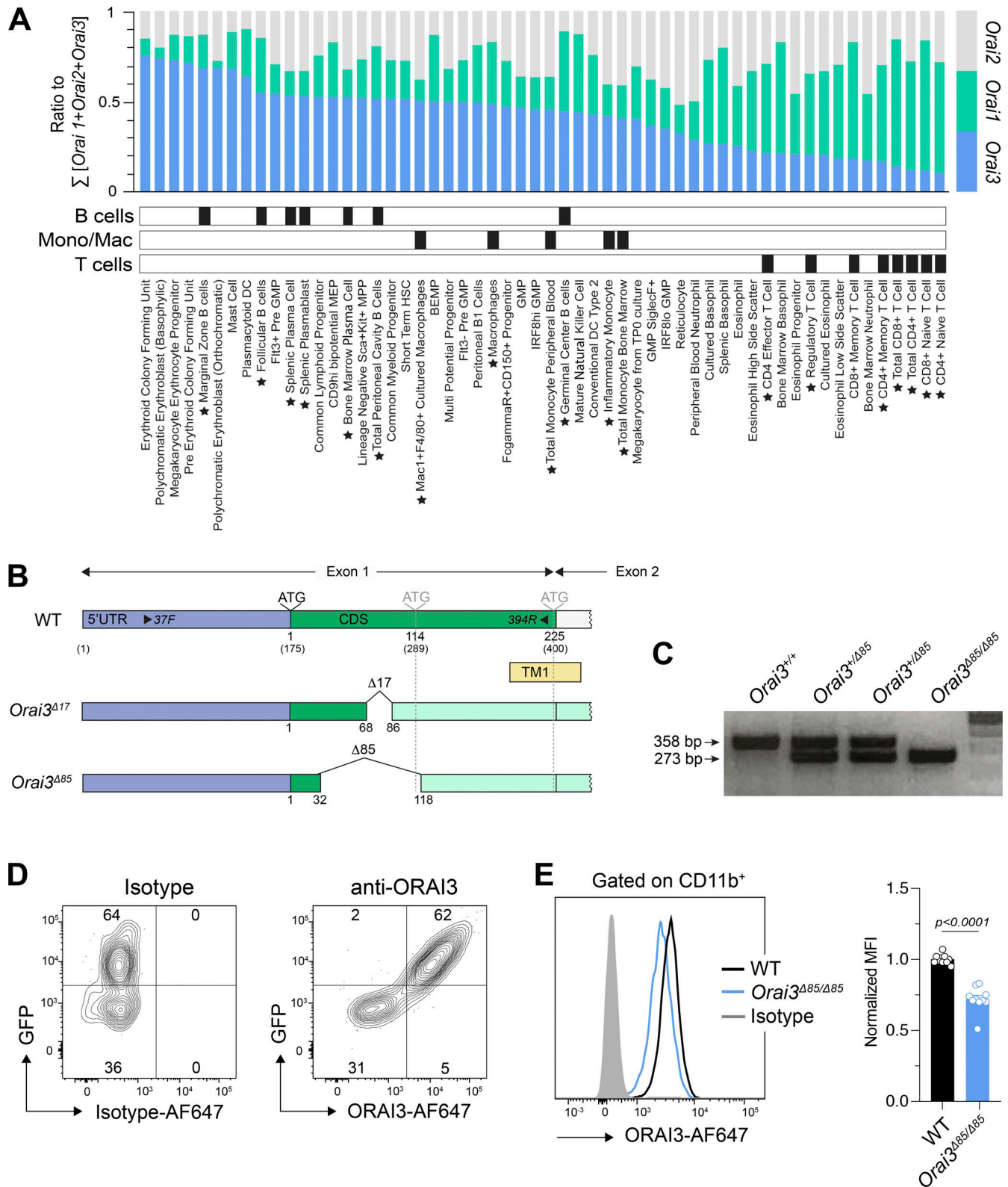
Figure 1. **Expression of *Orai3* in immune cells and generation of *Orai3⁻/⁻* mice. (A)** Analysis of mRNA expression levels of *Orai1*, *Orai2*, and *Orai3* in immune and hematopoietic cells extracted from the Haemopedia mouse RNA-seq dataset. TPM-normalized mRNA expression values for *Orai1*, *Orai2*, and *Orai3* were divided by their sum to obtain the relative expression of each homolog. Cell types were rank ordered according to relative expression of *Orai3*. Black boxes denote cell type categories. Stars next to cell type names denote B cells, macrophages, and T cells. **(B and C)** Generation of *Orai3*-knockout mice by CRISPR gene editing. **(B)** The positions of INDELs in exon of the *Orai3* gene found in *Orai3^Δ17^* and *Orai3^Δ85^* strains are indicated. ATG denotes the TIS for full-length ORAI3 protein (nt 1) and predicted alternative TIS (nt 114 and nt 225). Numbers in parentheses denote nt positions relative to the first nt of *Orai3* transcripts. 37F and 394R are the primers used for genotyping of mice. **(C)** Representative genotyping results of WT (*Orai3^+/+^*), *Orai3^+/Δ85^*, and *Orai3^Δ85/Δ85^* are shown.

(D) Detection of exogenously expressed ORAI3 protein by antibody staining. Plat-E cells were transfected with a bicistronic ORAI3 IRES-GFP plasmid. 48 h later, cells were fixed, permeabilized, and incubated with an anti-ORAI3 or isotype control antibody and analyzed by flow cytometry. One representative experiment is shown. **(E)** Detection of endogenously expressed ORAI3 in BMDMs. BMDMs from WT and $Orai3^{\Delta85/\Delta85}$ ($Orai3^{-/-}$) mice were stained with anti-ORAI3 or isotype control antibody. Shown are flow cytometry plots for one representative experiment (left) and the mean fluorescence intensity (MFI) ± SEM of 10 mice per genotype (right). Statistical analysis was performed by unpaired Student's t test; exact P values are indicated in each panel.

of 2 mM extracellular Ca^{2+}. WT BMDMs showed a small and sustained increase in intracellular Ca^{2+} in response to 2-APB, which was significantly smaller in BMDMs of $Orai3^{-/-}$ mice, suggesting that ORAI3 indeed mediates 2-APB–induced Ca^{2+} influx (Fig. S2 E). This finding further confirms the deletion of ORAI3 protein expression in $Orai3^{\Delta85}$ mice.

ORAI3 is not required for SOCE in B cells and B cell function in vitro

Because B cells have some of the highest ratios of $Orai3$ to ($Orai1 + Orai2$) mRNA expression compared with other immune cell types (Fig. 1 A), we investigated the role of ORAI3 in Ca^{2+} influx and B cell function. To directly test the role of ORAI3 in SOCE, we passively depleted ER Ca^{2+} stores with the SR/ER Ca^{2+} ATPase (SERCA) inhibitor TG. The peak, influx rate, and integrated area under the curve (AUC) of Ca^{2+} influx were moderately decreased in $Orai3$-deficient B cells, but this reduction reached statistical significance only for the AUC (Fig. S3 A). Antigen binding to BCR induces phospholipase $C\gamma2$ ($PLC\gamma2$) activation, IP_3 production, and SOCE. Because BCR crosslinking could potentially activate other Ca^{2+} influx pathways besides SOCE that might rely on ORAI3, we analyzed if deletion of ORAI3 in B cells isolated from the spleen of $Orai3^{-/-}$ mice affects Ca^{2+} influx. BCR crosslinking with different concentrations of anti-IgM antibodies resulted in a dose-dependent Ca^{2+} influx, whose peak amplitude and AUC were indistinguishable between WT and $Orai3^{-/-}$ mice (Figs. 2 A and S3 B). We conclude that ORAI3 is not a major contributor to SOCE or other BCR-induced forms of Ca^{2+} influx in B cells. We next investigated if ORAI3 is required for Ig class switching or the differentiation of B cells into antibody-producing plasma cells (PCs) in vitro. Naive B cells were stimulated in vitro with either LPS + IL-4 or feeder cells expressing CD40L and BAFF (40LB) in the presence of IL-4. Class switching from IgM to IgG1 induced by LPS + IL4 or the 40LB feeder cells was similar in WT and $Orai3^{-/-}$ B cells (Fig. 2 B). To evaluate the role of ORAI3 in PC differentiation, we stimulated naive B cells with 40LB and measured the frequencies of CD138$^+$ PCs. No differences in the frequencies of PCs were observed between WT and $Orai3^{-/-}$ mice (Fig. 2 C). These data indicate that ORAI3 is not required for Ig class switching and PC differentiation of mouse B cells in vitro. Near-complete suppression of SOCE by combined deletion of $Stim1$ and $Stim2$ was shown to impair B cell proliferation (Matsumoto et al., 2011; Berry et al., 2020). We therefore tested if deletion of $Orai3$ affects B cell expansion in vitro. Activation of naive B cells by BCR crosslinking, either alone or in combination with costimulatory signals, or by LPS stimulation resulted in robust proliferation of both WT and $Orai3^{-/-}$ B cells (Fig. 2 D). Collectively, these data demonstrate that ORAI3 is dispensable for SOCE and the function of B cells in vitro.

Normal B cell function and antibody responses in $Orai3^{-/-}$ mice in vivo

Because the magnitude of B cell activation by BCR crosslinking or TG stimulation in vitro is supraphysiological compared with B cell stimulation in vivo, we investigated the effects of $Orai3$ deletion on B cell development and function in vivo. The frequencies of pre- and pro-B cells as well as immature and mature B cells in the BM of WT and $Orai3^{-/-}$ mice were comparable (Fig. S4 A). In the spleen, the percentages of transitional B cells (T1, T2–3), follicular B cells, and marginal zone B cells were similar in WT and $Orai3^{-/-}$ mice (Fig. S4 B). Collectively, these findings show that $Orai3$ deletion does not affect murine B cell development. To address the role of ORAI3 in mature B cell function and B cell–mediated immune responses in vivo, we immunized WT and $Orai3^{-/-}$ mice with either T cell–independent (TI) or T cell–dependent (TD) antigens to investigate antibody production and affinity maturation of B cells. To assess TI antibody responses, mice were immunized with NP-conjugated Ficoll. 7 and 14 d after immunization, the serum titers of IgM and IgG antibodies were comparable in WT and $Orai3^{-/-}$ mice (Fig. S4 C). Moreover, no differences could be observed between WT and $Orai3$-deficient mice for either low-affinity (anti-NP_{25}) or high-affinity (anti-NP_4) IgM and IgG antibodies, suggesting that TI Ig class switch recombination and affinity maturation of B cells is independent of ORAI3. Production of most antigen-specific antibodies requires follicular T helper (Tfh) cells that provide germinal center (GC) B cells with costimulatory signals. To test if ORAI3 is required for TD antibody responses in vivo, we immunized mice with NP-conjugated KLH. 7 and 14 d after immunization, the serum titers of both low- and high-affinity IgM and IgG antibodies were comparable between WT and $Orai3^{-/-}$ mice (Fig. 2 E). Moreover, the frequencies and total numbers of Fas$^+$GL-7$^+$ GC B cells and B220^{low}CD138$^+$ PCs were comparable 14 d after immunization (Fig. 2 F). Taken together, these findings demonstrate that ORAI3 is not required for TI and TD antibody responses by B cells in vivo.

ORAI3 is dispensable for myeloid cell functions

Besides B cells, the $Orai3$ to ($Orai1 + Orai2$) mRNA expression ratio was highest in several subsets of murine myeloid cells including monocytes, macrophages, and pDCs (Figs. 1 A and S1). To test if deletion of $Orai3$ affects the development of macrophages and other myeloid cells in vivo, we analyzed their frequencies in different organs. The frequencies of CD11c$^+$ DCs, CD11b$^+$Ly6C$^+$ monocytes (Mo), CD11b$^+$Ly6G$^+$ neutrophils (Ne), and PDCA-1$^+$CD11c$^+$ pDCs in the BM (Fig. S5, A and B) and those of CD11b$^+$F4/80$^+$ macrophages in the peritoneal cavity (Fig. S5 C) were not altered in $Orai3^{-/-}$ mice compared with WT controls. The only exception was a reduced frequency of CD11c$^+$ DC in the peritoneal cavity of $Orai3^{-/-}$ mice.
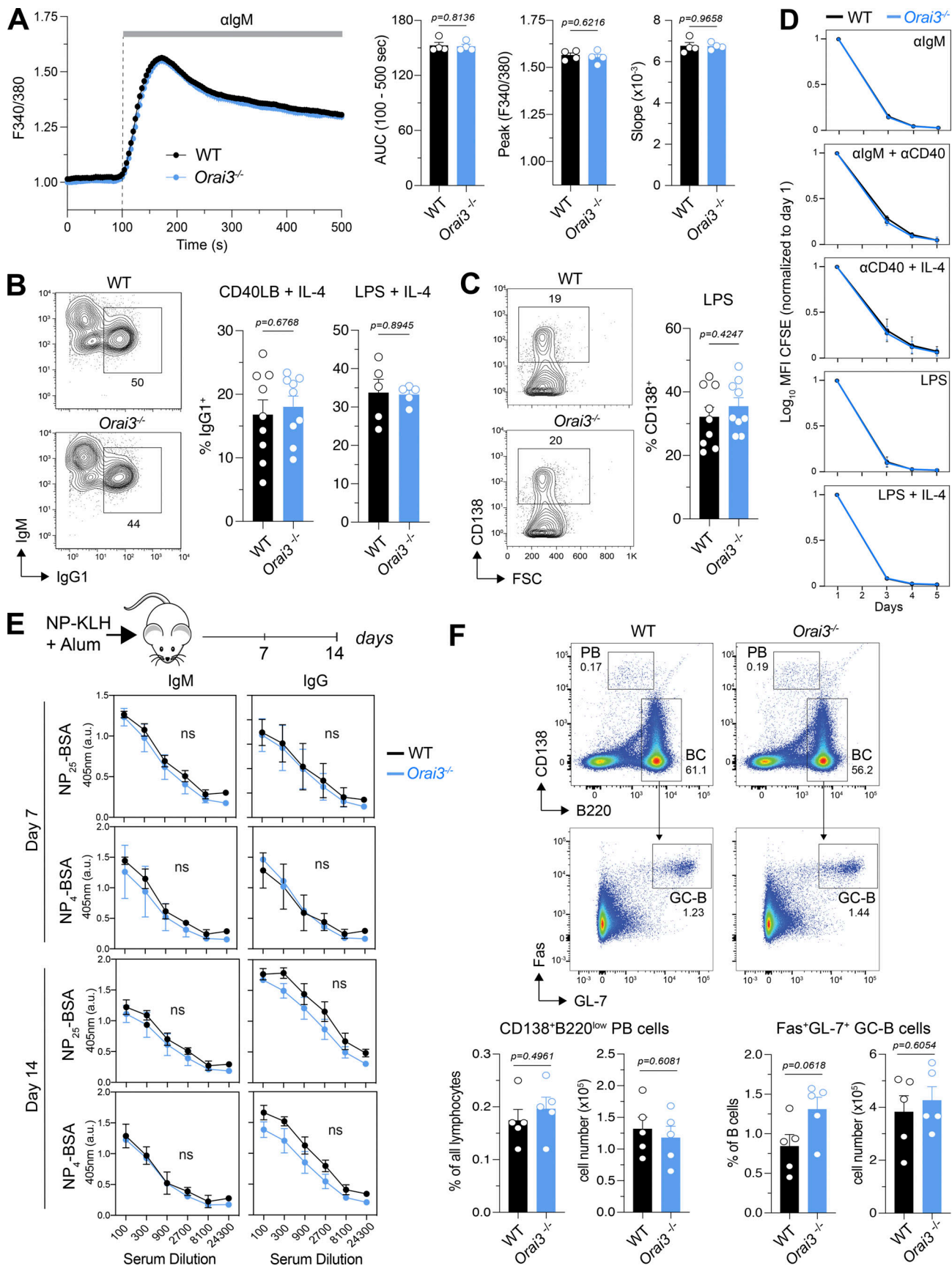
Figure 2. **ORAI3 is not required for B cell function in vitro or in vivo. (A)** Analysis of BCR crosslinking-induced Ca²⁺ influx in B cells. B220⁺ naive B cells were isolated from the spleens of WT and *Orai3⁻/⁻* mice, loaded with Fura-2-AM, and stimulated with 20 µg/ml anti-mouse IgM antibody in Ringer solution

containing 2 mM Ca^{2+}. Fura-2 signals were analyzed using a FlexStation 3 plate reader and normalized to the average Fura-2 ratios in the first 20 s. SOCE was analyzed as AUC, peak, and slope of Ca^{2+} rise. Shown are Ca^{2+} traces for one representative experiment (left) and the means ± SEM of four mice per group (right). **(B)** Analysis of class-switch recombination to IgG1 in B cells on day 4 after stimulation with LPS plus IL-4 or anti-CD40 plus IL-4. **(C)** Analysis of PC differentiation in B cells measured on day 4 after stimulation with LPS. Shown are flow cytometry plots for one representative experiment (left) and means ± SEM of nine mice per group. **(D)** Analysis of B cell proliferation. Dilution of CFSE was quantified, normalizing its mean fluorescence intensity (MFI) to day 1 after stimulation with the indicated mitogens. Shown are the means ± SEM of three to four mice per group. **(E)** Analysis of T cell–dependent B cell response in vivo. Serum was collected on days 7 and 14 after immunization with NP-KLH in alum adjuvant. ELISA was performed to detect antibody levels of low affinity (binding to NP$_{25}$-BSA) and high affinity (binding to NP$_4$-BSA) NP-specific IgM and IgG. Shown are means ± SEM of five mice per group. **(F)** Analysis of frequency and total cellularity of plasma B cell (B220^{low}CD138$^+$) and germinal center B cell (Fas$^+$GL7$^+$B220$^+$) in spleens of mice on day 14 after immunization with NP-KLH in alum adjuvant. Shown are the means ± SEM of five mice per group. Statistical analysis was performed by unpaired Student's *t* test; exact P values are indicated in each panel.

To test if ORAI3 is required for SOCE in macrophages, we generated BMDMs from WT and *Orai3*$^{-/-}$ mice. On day 7 of differentiation in vitro, we observed similar frequencies of CD11b$^+$ cells from WT and *Orai3*$^{-/-}$ mice, suggesting that deletion of *Orai3* does not affect BMDM differentiation in vitro (not depicted). FcR crosslinking by increasing concentrations of FcR antibody resulted in dose-dependent increases in Ca^{2+} influx that were, however, comparable in WT and *Orai3*$^{-/-}$ BMDMs (Figs. 3 A and S6 A). Direct induction of SOCE by passive depletion of ER Ca^{2+} stores with ionomycin (Fig. 3 A) or TG (Fig. 3 B) resulted in a moderate but significant increase in [Ca^{2+}]$_i$ in *Orai3*$^{-/-}$ BMDMs compared with WT cells. Increased SOCE in *Orai3*-deficient BMDMs is reminiscent of similar findings in BMDMs from *Orai2*$^{-/-}$ mice (Vaeth et al., 2017a), suggesting that ORAI3 may inhibit CRAC channel function, at least under conditions of maximal store depletion. ORAI3 has been reported to form heteropentameric ARC channels comprising two ORAI3 and three ORAI1 subunits (Shuttleworth et al., 2004; Hoth and Niemeyer, 2013). Unlike the CRAC channel, the ARC channel is activated by AA in a store-independent manner. We therefore investigated if AA-induced Ca^{2+} influx through ARC channels is observable in BMDMs and whether it is reduced in cells of *Orai3*$^{-/-}$ mice. We treated WT and *Orai3*$^{-/-}$ BMDMs with a range of AA concentrations (0–20 µM), which have been reported to elicit ARC channel activation in HEK293 cells and in murine parotid and acinar cells, but failed to observe AA-induced Ca^{2+} influx in WT or *Orai3*$^{-/-}$ BMDMs (Fig. S6, B and C). We conclude that ORAI3 does not form ARC channels in macrophages.

ORAI3 is highly expressed in a particular subtype of DCs, pDCs (Figs. 1 A and S1 A). The main function of this rare immune cell type is to secrete large quantities of type 1 IFNs in response to infection. To test if ORAI3 is involved in pDC function, we stimulated total bone marrow of WT and *Orai3*$^{-/-}$ mice with the TLR9 agonist CpG-A that mimics infection by viruses and bacteria (Guiducci et al., 2006). We did not observe differences in the amount of IFNα produced in response to CpG-A stimulation of bone marrow from WT and *Orai3*$^{-/-}$ mice (Fig. S7 A). Because pDCs are by far the most potent producers of IFNα, we conclude that deletion of ORAI3 does not affect pDC function.

Macrophages play essential roles in immunity to infections, tissue inflammation, antitumor immunity, and many other immune responses. These divergent roles are associated with both pro- and anti-inflammatory properties of macrophages. BMDMs can be differentiated in vitro from nonpolarized M0 cells into proinflammatory M1 macrophages (in the presence of LPS and IFNγ) that produce TNFα, IL-6, and nitric oxide (NO) and regulatory M2 macrophages (in the presence of IL-4 and IL-13) that express arginase-1 and other signature genes. To evaluate if ORAI3 determines the polarization and function of pro- and anti-inflammatory macrophages, we measured the protein expression of NOS2 and arginase-1 in M1 and M2 macrophages. *Orai3*-deficient and WT M1 macrophages showed a similar upregulation of NOS2 expression; likewise, arginase-1 expression was comparable in M2 macrophages (Fig. 3 C). LPS and IFNγ also resulted in the strong upregulation of *Nos2*, *Il6*, and *Tnfa* mRNA expression, as well as CD80 and PD-L1 protein expression in M1 macrophages, which were comparable between WT and *Orai3*$^{-/-}$ mice (Fig. S7, B and C). Moreover, the expression of *Arg1*, *Chi3l3*, and *Retnla* mRNA was unaltered in *Orai3*-deficient M2 macrophages (Fig. S7 B). Stimulation of BMDMs with LPS results in the NF-κB–dependent induction of the NLRP3 (NOD-, LRR-, and pyrin domain–containing protein 3) inflammasome, which mediates the production of IL-1β or IL-18 in response to a variety of inflammatory stimuli and causes pyroptosis, a highly inflammatory form of cell death (Man et al., 2017). To test if ORAI3 is involved in inflammasome function, we treated BMDMs with LPS for 4 h followed by acute stimulation with ATP. Treatment of WT and *Orai3*-deficient BMDMs with LPS and ATP induced similar levels of IL-1β (Fig. S7 D), suggesting that ORAI3 is not required for ATP-induced inflammasome function. Whereas LPS activates TLR4, macrophages also express other pattern recognition receptors that detect molecules from pathogens or damaged cells (Takeuchi and Akira, 2010; Amarante-Mendes et al., 2018; Li and Wu, 2021). Stimulation of BMDMs with the pattern recognition receptor agonists LPS, imiquimod (TLR7), or Zymosan (Dectin-1) resulted in similar levels of *Tnfa* and *Il6* expression in WT and *Orai3*-deficient cells (Fig. 3 D). Macrophages, like many other cell types, are able to sense the presence of intracellular DNA and RNA, which are detected by the DNA sensor cGAS and the RNA sensors retinoic acid–inducible gene I (RIG-I) and TLR3 (Perales-Linares and Navas-Martin, 2013), respectively, and which induce a type I IFN response (Chan and Gack, 2016; Yu and Liu, 2021). Stimulation of BMDMs with synthetic DNA (poly(dA:dT)) or RNA (poly(I:C)) mimetics induced the expression of IFNβ to a similar degree in WT and *Orai3*$^{-/-}$ BMDMs (Fig. S7 E). These data demonstrate that *Orai3* deletion does not alter several important effector functions of BMDMs in vitro despite increased SOCE in the absence of ORAI3.

Because BMDMs may not properly represent macrophages in vivo, we tested whether deletion of *Orai3* impairs
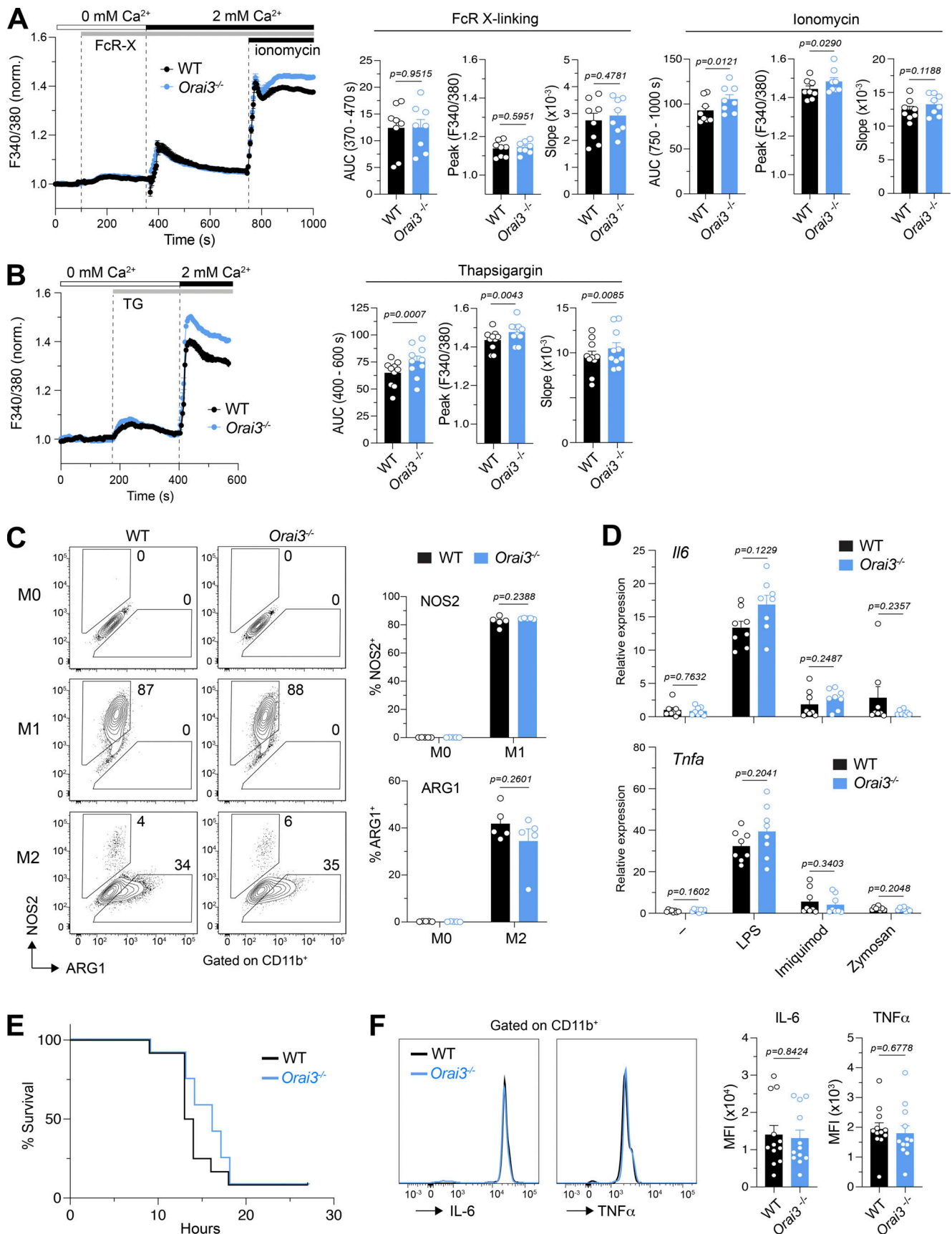
Figure 3. **ORAI3-deficient macrophages have increased SOCE, but normal macrophage function. (A and B)** Analysis of SOCE in BMDMs. BMDMs from WT and *Orai3⁻/⁻* mice were differentiated for 7 d in L929 medium. BMDMs were loaded with Fura-2-AM, and Ca²⁺ signals were measured with a FlexStation 3

plate reader. Ca^{2+} store depletion was induced by incubating BMDMs with 10 µg/ml anti-CD16/CD32 followed by FcR cross-linking with 30 µg/ml goat anti-rat IgG antibody (A) and 1 µM TG (B) in Ca^{2+}-free buffer. SOCE was induced by readdition of Ringer solution containing 2 mM extracellular Ca^{2+}. Maximal SOCE was induced by 1 µM ionomycin. SOCE was analyzed as the AUC, peak, and slope of Ca^{2+} rise. Shown are Ca^{2+} traces for one representative experiment (left) and means ± SEM of eight to nine mice per group. **(C)** Analysis of BMDM polarization into M1 and M2 macrophages. BMDMs were left untreated (M0) or stimulated with LPS + IFNγ (M1) or IL-4 + IL-13 (M2) for 24 h. The expression of NOS2 and ARG1 on CD11b$^+$ BMDMs was measured by flow cytometry. Shown are flow cytometry plots for one representative experiment (left) and means ± SEM of five mice per genotype. **(D)** BMDMs were stimulated with 100 ng/ml LPS, 1 µg/ml Imiquimod, or 20 µg/ml Zymosan for 18 h or left untreated (mock). Expression of *IL6* and *TNFa* measured by qRT-PCR in the macrophages. Shown are means ± SEM of eight mice per genotype. **(E and F)** Induction of septic shock. **(E)** Survival of mice after induction of septic shock with 54 mg/kg LPS i.p. **(F)** Relative levels of IL-6 and TNFα in serum 6 h after induction of septic shock, measured by CBA. Shown are representative flow cytometry plots (left) and means ± SEM of 12 mice per genotype (right). Statistical analysis in A and B was performed by paired Student's *t* test. Statistical analysis in C, D, and F was performed by unpaired Student's *t* test; exact P values are indicated in each panel.

macrophage-dependent immune responses in mice. Septic shock is a life-threatening inflammatory process during which monocytes differentiate into inflammatory M1 macrophages and produce proinflammatory cytokines such as TNFα, IL-6, IL-1β, and reactive oxygen species (ROS) including NO, which cause systematic inflammation and organ failure (Cheng et al., 2018). Given the important role of macrophages in sepsis, we investigated if *Orai3*$^{-/-}$ mice show an altered susceptibility to septic shock. *Orai3*$^{-/-}$ mice succumbed to i.p. LPS injection at a similar rate and with similar kinetics as WT mice (Fig. 3 E). Moreover, serum levels of TNFα and IL-6, two essential cytokines in sepsis, were comparable in WT and *Orai3*$^{-/-}$ mice (Fig. 3 F). Taken together, these results suggest that ORAI3 is dispensable for macrophage functions in vitro and in vivo.

ORAI3 is not required for SOCE in T cells and is dispensable for T cell function in vitro

Compared with B cells and macrophages, T cells have lower *Orai3* mRNA levels relative to *Orai1* and *Orai2*, which does not, however, exclude a potential function of ORAI3 in T cells. In human T cells, ORAI3 was reported to be upregulated in CD4$^+$ effector T cells and to confer resistance to suppression of SOCE by H$_2$O$_2$ (Bogeski et al., 2010). Moreover, ORAI3 was shown to be upregulated and form Ca^{2+}-permeable, AA-activated ARC channels in T cells isolated from patients with RA (Ye et al., 2021). We therefore investigated if ORAI3 plays a role in the development and function of T cells in vitro and in vivo. T cell development in the thymus of *Orai3*$^{-/-}$ mice was normal compared to littermate controls (Fig. S8 A). The frequencies of CD4$^+$ and CD8$^+$ T cells in the spleen were unchanged, including the distribution of CD62L$^+$CD44$^-$ naive and CD62L$^-$CD44$^+$ effector T cells (Fig. S8, B and C). Moreover, we did not detect significant differences in the frequencies of CD4$^+$Foxp3$^+$ Treg cells in *Orai3*$^{-/-}$ mice compared to controls (Fig. S8 D). These data indicate that T cell development is intact in the absence of ORAI3.

To assess whether ORAI3 regulates SOCE in T cells, as was demonstrated for ORAI1 and ORAI2 (Vaeth et al., 2017a), we stimulated T cells by TCR crosslinking and by direct ER store depletion. TCR stimulation of CD4$^+$ T cells by anti-CD3ε crosslinking induced comparable Ca^{2+} influx in WT and *Orai3*$^{-/-}$ cells (Fig. 4 A). Subsequent treatment with ionomycin to induce SOCE enhanced Ca^{2+} levels to a similar degree in T cells from both mice. The magnitude of SOCE in CD4$^+$ T cells in response to passive ER store depletion with TG was also similar in WT and *Orai3*$^{-/-}$ cells (Fig. S9 A). Collectively, these data indicate that

ORAI3 is either not required or is redundant for SOCE in murine T cells, at least under supraphysiological stimulation conditions.

One of the main functions of Ca^{2+} influx in T cells is the regulation of gene expression, including cytokines and metabolic enzymes, which in turn controls T cell function (Vaeth et al., 2020). Ca^{2+}-dependent gene expression requires sustained Ca^{2+} signals over several hours. Ca^{2+} signals, including the ones described above, however, are typically recorded for only several minutes and may not reveal differences in prolonged Ca^{2+} influx in the absence of ORAI3. We therefore investigated whether the differentiation and function of T cells, which requires prolonged SOCE, is altered in the absence of ORAI3. Naive CD4$^+$ T cells were stimulated and polarized in vitro into Th cell subsets and induced Treg (iTreg) cells, which express transcription factors and cytokines that are cell type specific. Deletion of *Orai3* did not affect the frequency of IFNγ-producing Th1 cells, IL-13–producing Th2 cells, and IL-17A–producing Th17 cells (Fig. 4 B). Likewise, expression levels of the subset-specific transcription factors T-bet, GATA3, and RORγt were comparable in Th1, Th2, and Th17 polarized cells, respectively (Fig. 4 C). The frequencies of Foxp3$^+$ iTreg cells that were induced following incubation of naive CD4$^+$ T cells with TGFβ were also similar in the presence or absence of ORAI3 (Fig. 4 D). SOCE is critical for the proliferation and clonal expansion of human and mouse T cells (Vaeth et al., 2017a). To evaluate the role of ORAI3 in T cell proliferation, we stimulated CD4$^+$ splenic T cells from WT and *Orai3*$^{-/-}$ mice in vitro. 72 h after activation, the number of T cells that had undergone cell division was not altered in the absence of ORAI3 (Fig. 4 E).

The gene expression studies described above were conducted in CD4$^+$ T cells. Cytotoxic CD8$^+$ T cells play important roles in immunity to viral infections and tumors. Their function requires SOCE because ablation of *Stim1* and *Stim2* in CD8$^+$ T cells impairs antiviral and antitumor immunity in vivo (Weidinger et al., 2013; Shaw et al., 2014), and deletion of *Orai1* impairs the cytotoxic function of CD8$^+$ T cells (Kaschek et al., 2021). We therefore tested the effects of *Orai3* deletion on SOCE and the function of CD8$^+$ T cells. Ca^{2+} influx induced by TCR crosslinking was similar in WT and *Orai3*$^{-/-}$ CD8$^+$ T cells that had been cultured in vitro for 5 d (Fig. 5 A). Neither did we observe significant differences in SOCE induced by passive ER store depletion with either ionomycin or TG treatment (Figs. 5 A and S9 B). As is the case for CD4$^+$ T cells, the expression of effector cytokines by CD8$^+$ T cells depends on SOCE. Costimulation of in vitro–expanded CD8$^+$ T cells with ionomycin, to induce SOCE, and
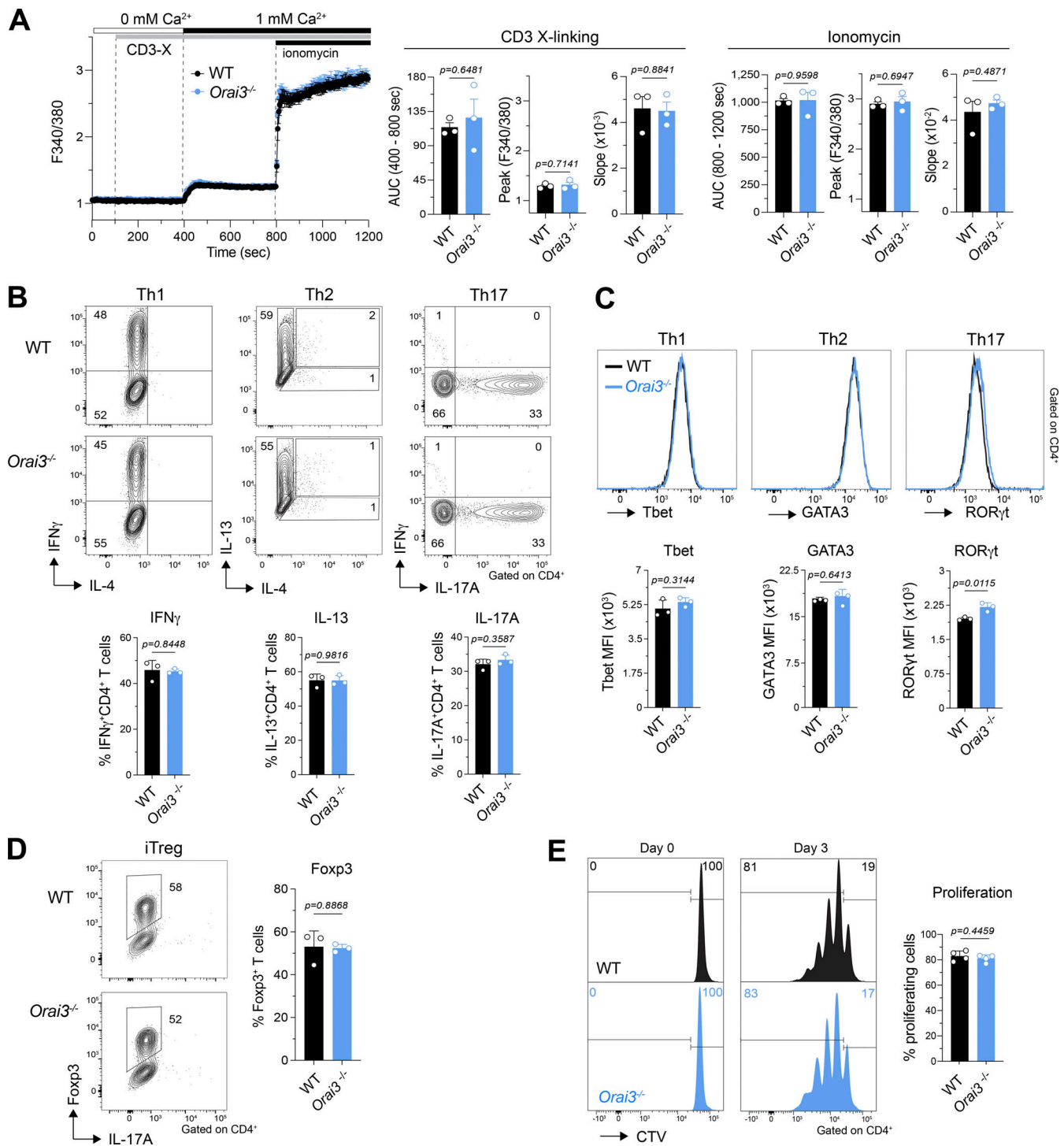
Figure 4. **ORAI3 is not required for SOCE and is dispensable for cell proliferation and differentiation in CD4+ T cells. (A)** Analysis of SOCE in CD4+ T cells. CD4+ T cells isolated from spleens of WT and *Orai3*−/− mice were activated with plate-bound anti-CD3/CD28 for 4 d in vitro, loaded with Fura-2-AM, and analyzed for Ca2+ signals using a FlexStation 3 plate reader. Ca2+ store depletion was induced by incubating cells with 1 µg/ml anti-CD3ε antibody for 30 min followed by TCR cross-linking with 1 µg/ml rabbit anti-hamster IgG in Ca2+-free buffer. SOCE was induced by readdition of Ringer solution containing 1 mM extracellular Ca2+. Maximal SOCE was induced with 1 µM ionomycin. SOCE was analyzed as AUC, peak, and slope of Ca2+ rise. Shown are Ca2+ traces for one representative experiment (left) and means ± SEM of three mice per group (right). **(B–D)** Analysis of Th1, Th2, Th17, and Treg cell differentiation in WT and *Orai3*−/− CD4+ T cells. **(B)** T cells isolated from WT and *Orai3*−/− mice were differentiated for 3 d under Th1, Th2, Th17, and Treg cell polarizing conditions, and intracellular IFNγ, IL-13, IL-4, and IL-17 were analyzed by flow cytometry after restimulation with PMA/ionomycin for 6 h. **(C and D)** The same T cells from B were analyzed for transcription factors Tbet, GATA3, RORγt, and Foxp3 by flow cytometry. Shown are flow cytometry plots for one representative experiment and means ± SEM of three mice per genotype. **(E)** Analysis of cell proliferation in Orai3-deficent CD4+ T cells. Splenocytes isolated from WT and Orai3−/− mice were stimulated with plate-bound anti-CD3/CD28 for 3 d in vitro. CD4+ T cells proliferation was analyzed by CTV dilution using flow cytometry. Shown are flow cytometry plots for one representative experiment (left) and mean fluorescence intensity (MFI) ± SEM of four mice per genotype (right). Statistical analysis was performed by unpaired Student's *t* test; exact P values are indicated in each panel.

PMA induced robust expression of the cytokines IL-2, TNFα, IFNγ, and the serine protease granzyme B in WT and *Orai3*-deficient T cells (Fig. 5 B). Moreover, CD8^{+} T cells from *Orai3*^{−/−} mice proliferated normally compared with WT T cells when stimulated with anti-CD3/anti-CD28 antibodies for 3 d (Fig. 5 C). Collectively, these data indicate that ORAI3 is dispensable for cytotoxic CD8^{+} T cell function in vitro.

ORAI3 is dispensable for CD8^{+} T cell–dependent antitumor immunity in vivo

We considered the possibility that ORAI3 may play a role in T cell–mediated immunity in vivo under more physiological stimulation conditions. TCR stimulation by antigens in vivo is weaker than TCR crosslinking in vitro. Moreover, T cell activation occurs in tissue- and disease-specific microenvironments that are enriched in cytokines, ROS, and other inflammatory factors. We therefore investigated if deletion of *Orai3* affects CD8^{+} T cell–dependent antitumor immunity in vivo. To this end, we crossed *Orai3*^{−/−} mice to OT-I mice that express a transgenic TCR that recognizes OVA peptide presented by MHC class I molecules on tumor cells. We isolated CD8^{+} T cells from *Orai3*^{−/−} OT-I mice, differentiated them into CTLs, and injected them into host mice that had been implanted with melanoma cells expressing OVA (B16-OVA) 10 d earlier (Fig. 5 D). Tumor growth in the host mice was biphasic: 5 d after T cell transfer, the tumors became smaller, likely because of effective tumor killing by the injected CTLs; at 15 d after T cell transfer, the tumors began to grow again, potentially due to CTL exhaustion. Importantly, the kinetics of tumor growth and the sizes of tumors were similar in host mice that had received WT OT-I CD8^{+} T cells or *Orai3*^{−/−} OT-I CD8^{+} T cells (Fig. 5 D). It is noteworthy that even when the experiment was repeated in a competitive setting during which WT OT-I and *Orai3*^{−/−} OT-I CD8^{+} T cells were cotransferred into tumor-bearing host mice at a 1:1 ratio to unmask a putative functional defect of *Orai3*-deficient T cells, the numbers of tumor-infiltrating *Orai3*-deficient CTLs were comparable to those of WT CTLs (Fig. 5 E). These findings demonstrate that ORAI3 is not required for antitumor immunity mediated by CD8^{+} T cells in vivo and their ability to infiltrate tumors or persist in the tumor microenvironment.

### ORAI3 is not required for T cell–dependent autoimmunity in vivo

CD4^{+} T cells are critical mediators of autoimmunity in many forms of autoimmune diseases including type 1 diabetes, multiple sclerosis (MS), RA, and inflammatory bowel disease (IBD). The function of autoreactive T cells depends on SOCE because deletion of *Orai1* or *Stim1* in mouse models of MS and IBD significantly attenuates disease severity (Ma et al., 2010; McCarl et al., 2010; Schuhmann et al., 2010; Kaufmann et al., 2016; Vaeth et al., 2017b). We first tested the effects of *Orai3* deletion in EAE, a T cell–dependent mouse model of MS (Rangachari and Kuchroo, 2013). In addition to T cells, B cells, macrophages, neutrophils, and other immune cells also contribute to EAE pathology (Caravagna et al., 2018; Chu et al., 2018; Pierson et al., 2018). We hypothesized that deletion of *Orai3* may impair the function of CD4^{+} T cells, and potentially other immune cells, and

result in altered severity of EAE. Immunization of mice with MOG peptide induced severe paralysis in WT and *Orai3*^{−/−} mice. The incidence, kinetics, and severity of disease were similar in WT and *Orai3*^{−/−} mice (Fig. 6, A and B). Moreover, the numbers of CNS-infiltrating immune cells, including CD4^{+} and CD8^{+} T cells, Th17 cells, Treg cells, neutrophils, and B cells were similar in WT and *Orai3*^{−/−} mice (Fig. 6 C). We conclude that ORAI3 is dispensable for the ability of CD4^{+} T cells (and other immune cells) to induce CNS inflammation in the context of EAE.

ORAI3 may be involved in the pathophysiology of RA. Its expression was reported to be increased in CD4^{+} T cells from RA patients (Ye et al., 2021). Deletion of ORAI3 in T cells of RA patients before their injection into immunodeficient mice attenuated synovitis. Another study showed that systemic injection of mice with shRNAs targeting *Orai3* mRNA attenuated CIA in a rodent model of RA (Liu et al., 2015). In this study, we induced CIA in WT and *Orai3*^{−/−} mice and monitored joint inflammation. The times to disease onset and maximum RA scores were moderately reduced in *Orai3*^{−/−} mice compared with WT littermates, whereas the disease incidence was increased in *Orai3*^{−/−} mice (Fig. 6, D and E). These differences did not, however, reach statistical significance. Macroscopic joint swelling was comparable in WT and *Orai3*^{−/−} mice (Fig. 6 F). The histological analysis of WT and *Orai3*^{−/−} mice revealed a similar degree of synovitis, pannus formation, and bone erosion (Fig. 6, G and H). CIA is associated with the formation of anti-collagen antibodies. The levels of collagen-specific IgG antibodies were comparable in WT and *Orai3*^{−/−} mice (Fig. 6 I). Moreover, the frequencies of plasma cells and germinal center B cells in the draining inguinal lymph nodes were unchanged in *Orai3*^{−/−} mice (Fig. S10 A). TNFα and IL-6 are critical proinflammatory cytokines in RA pathology and the targets of disease-modifying drugs. We found comparable levels of IFNγ, TNFα, and IL-6 in the serum as well as similar production of IFNγ and TNFα by CD4^{+} and CD8^{+} T cells isolated from the draining LNs of WT and *Orai3*^{−/−} mice (Fig. 6 J; and Fig. S10, B and C). Because Ca^{2+} influx was reported to be altered in *ORAI3*-deficient human CD4^{+} T cells only in the context of RA but not under noninflamed conditions (Liu et al., 2015), we measured SOCE in CD4^{+} T cells isolated from the spleen of WT and *Orai3*^{−/−} mice 56–59 d after induction of CIA. TG stimulation resulted in similar levels of SOCE in *Orai3*-deficient CD4^{+} T cells compared to WT controls (Fig. 6 K). Neither did we observe differences in SOCE between splenic CD8^{+} T cells and B cells from WT and *Orai3*^{−/−} mice with CIA (Fig. S10, D and E). Taken together, our data demonstrate that ORAI3 does not play a role in the pathophysiology of CIA and EAE. Because multiple immune cell types including T cells, B cells, and macrophages are involved in disease initiation and progression in both autoimmune diseases, we conclude that despite its expression in these immune cells, ORAI3 is dispensable for their function.

Discussion

SOCE is a major Ca^{2+} influx pathway in lymphoid and myeloid immune cells. Of the three CRAC channel-forming proteins,
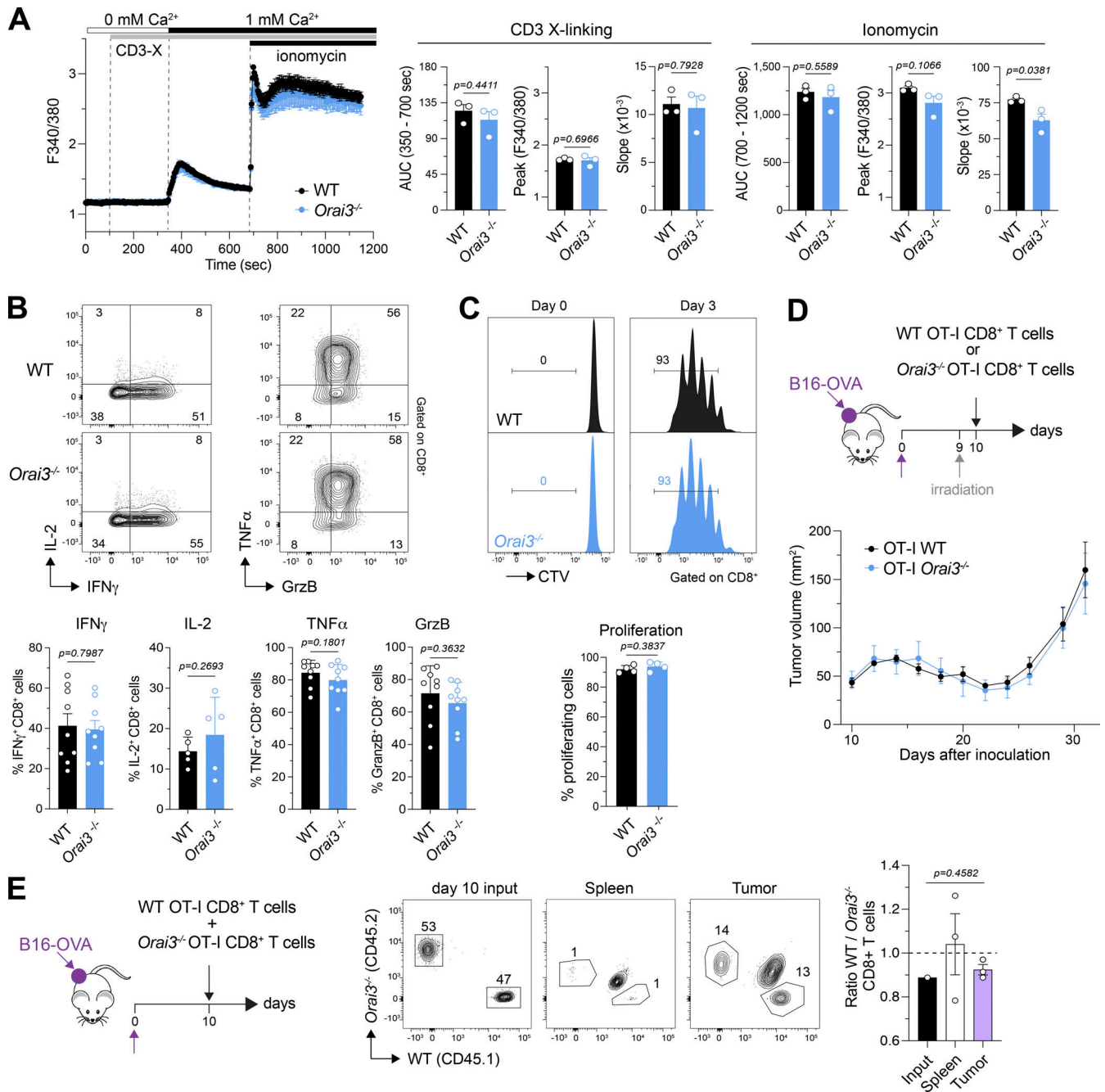
Figure 5. ORAI3 is not required for SOCE and is dispensable for cell proliferation and differentiation for CD8+ T cells. (A) Analysis of SOCE in CD8+ T cells. Naive CD8+ T cells isolated from spleens of WT and *Orai3*−/− mice were activated with plate-bound anti-CD3/CD28 for 2 d and expanded in IL-2 for an additional 3 d in vitro. Cells were loaded with Fura-2-AM, and Ca2+ signals were measured using with a FlexStation 3 plate reader. Ca2+ store depletion was induced by incubating cells with 1 µg/ml anti-CD3ε antibody for 30 min followed by TCR cross-linking with 1 µg/ml rabbit anti-hamster IgG in Ca2+-free buffer. SOCE was induced by readdition of Ringer solution containing 1 mM extracellular Ca2+. Maximal SOCE was induced with 1 µM ionomycin. SOCE was analyzed as AUC, peak, and slope of Ca2+ rise. Shown are Ca2+ traces for one representative experiment (left) and means ± SEM of three mice per group (right). **(B)** Analysis of cytokine and granzyme B production in WT and Orai3-deficient CD8+ T cells. Intracellular IFNγ, IL-2, TNFα, and Granzyme B in CD8+ T cells from A were analyzed by flow cytometry after restimulation with PMA/ionomycin for 6 h. Shown are flow cytometry plots for one representative experiment (top) and mean frequencies ± SEM of five to nine mice per genotype (bottom). **(C)** Analysis of cell proliferation in WT and *Orai3*-deficient CD8+ T cells. Splenocytes isolated from WT and *Orai3*−/− mice were stimulated with plate-bound anti-CD3/CD28 for 3 d in vitro. CD8+ proliferation was analyzed by CTV dilution using flow cytometry. Shown are flow cytometry plots for one representative experiment (left) and mean fluorescence intensity (MFI) ± SEM of four mice per genotype (right). **(D–E)** ORAI3 in CD8+ T cell–mediated antitumor immunity. **(D)** OT-I T cells isolated from WT and *Orai3*−/− mice were cultured in vitro for 4 d and injected i.v. into tumor-bearing mice on day 10 after engraftment of B16-OVA melanoma, followed by analyses of tumor size. Shown are means ± SEM of six mice for each genotype. **(E)** OT-I cells isolated from WT and *Orai3*−/− mice were cultured in vitro for 4 d, mixed at a 1:1 ratio, and injected i.v. into tumor-bearing mice. After 10 d, donor OT-I cells were isolated from spleens and tumors and analyzed by flow cytometry. Shown are means ± SEM of three mice from one experiment. Data are representative of two independent experiments. Statistical analysis in B was performed by paired Student's *t* test. Statistical analysis in A, C, and E was performed by unpaired Student's *t* test.; exact P values are indicated in each panel.
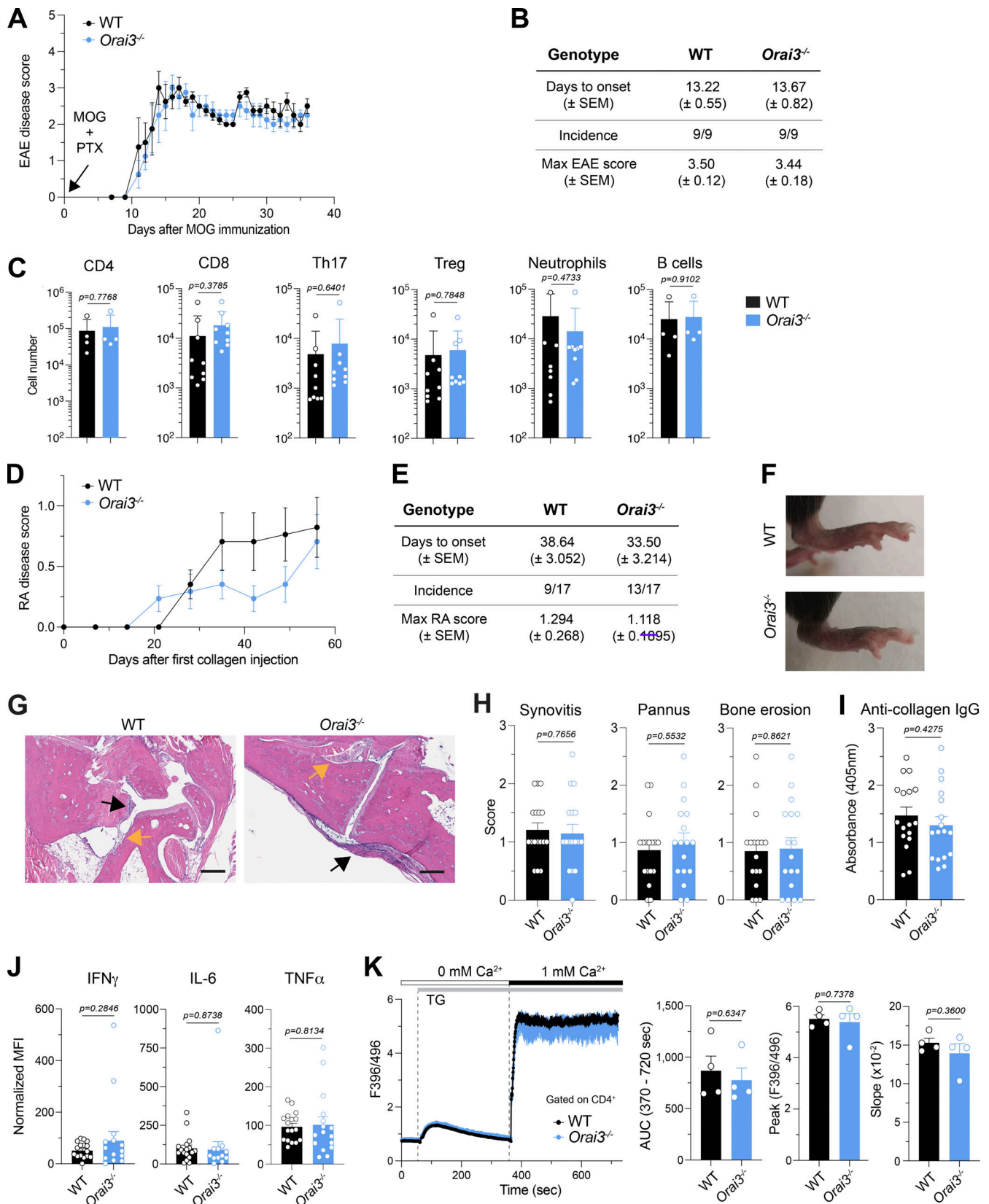
Figure 6. **ORAI3 is dispensable for the development of EAE and CIA. (A)** Disease scores of EAE in WT and *Orai3*^{−/−} mice immunized with MOG[35–55] in CFA followed by PTX injection. **(B)** Summary of EAE in WT and *Orai3*^{−/−} mice by days to onset (± SEM), incidence, and maximal disease score (± SEM). **(C)** Analysis of immune cells isolated from the spinal cord of WT and *Orai3*^{−/−} mice 36 d after EAE induction. Shown are absolute numbers of CD4^{+} and CD8^{+} T cells, RORγt^{+}CD4^{+} Th17 cells, Foxp3^{+}CD4^{+} Treg cells, CD11b^{+}Gr-1^{+} neutrophils, and B220^{+} B cells in the CNS of mice measured by flow cytometry. **(D)** Disease scores

of CIA in WT and *Orai3⁻/⁻* mice. **(E)** Summary of CIA in WT and *Orai3⁻/⁻* mice by days to onset, incidence, and maximal disease score. Shown are means ± SEM of 17 mice per genotype. **(F)** Representative images of hind paws of WT and *Orai3⁻/⁻* mice with CIA. **(G and H)** Representative H&E staining of hind paw sections and histology scores for synovitis, pannus formation, and bone erosion in WT and *Orai3⁻/⁻* mice with CIA. Black arrows indicate synovitis and pannus formation, and yellow arrows indicate bone erosion. The scale bar represents 200 µm. **(I)** Serum levels of anti-collagen IgG measured by ELISA. **(J)** Cytokine levels in the serum of WT and *Orai3⁻/⁻* mice 56–59 d after CIA induction and analyzed by CBA. Normalized mean fluorescence intensity (MFI) was calculated as the MFI of a sample (serum) minus the MFI of blank (PBS). Data are from 12 to 17 mice per genotype. **(K)** Analysis of SOCE in splenic $CD4^+$ T cells isolated from WT and *Orai3⁻/⁻* mice 56–59 d after CIA induction. T cells were stimulated with 1 µM TG in Ca^{2+}-free buffer followed by readdition of 1 mM extracellular Ca^{2+}. SOCE was analyzed as AUC, peak, and slope of the Ca^{2+} rise. Shown are representative Ca^{2+} traces (left) and means ± SEM of four mice per group (right). Statistical analysis was performed by unpaired Student's *t* test. Exact P values are indicated in each panel.

ORAI1 is the best characterized, whereas the physiological role of ORAI3 in immune cells is not known. Loss-of-function mutations in human *ORAI1* abolish SOCE and cause immunodeficiency (Feske et al., 2006; Lacruz and Feske, 2015; Vaeth and Feske, 2018). Genetic deletion of *Orai1* in murine T cells reduces SOCE and affords protection against T cell–dependent autoimmunity in preclinical models of MS and IBD. Combined deletion of both *Orai1* and *Orai2* abolishes SOCE in T cells and neutrophils and strongly impairs their function (Grimes et al., 2020), demonstrating that ORAI2 contributes to CRAC channel function and SOCE in mouse immune cells. A similar role for ORAI3 has not yet been shown.

We here demonstrate that *Orai3* mRNA is highly expressed in murine macrophages and B cells, and to a lesser degree also in T cells. Genetic deletion of *Orai3*, however, only affected SOCE in macrophages after passive depletion of ER Ca^{2+} stores, but not in other immune cells. The development of these immune cells and their function in vitro were unaffected by the loss of *Orai3*. Moreover, the deletion of *Orai3* had no effect on the development of B cells and their function in vivo, specifically the production of IgM and IgG antibodies after immunization. *Orai3* deletion did not have a protective effect in an LPS-induced model of septic shock, which depends on the function of inflammatory macrophages. Neither did the lack of *Orai3* expression affect the function of T cells in several models of T cell–dependent immune responses. $CD8^+$ T cell–mediated antitumor immunity in a xenograft melanoma model was normal in *Orai3⁻/⁻* mice, and $CD4^+$ T cells lacking ORAI3 were able to cause CNS and joint inflammation in mouse models of MS and RA. Although each model aimed to investigate ORAI3 function in one type of immune cell, immune responses are dependent on the cross-talk between multiple immune cell subsets. Antibody production requires the synergistic function of T and B cells in germinal centers; antitumor immunity is mediated by $CD8^+$ T cells, macrophages, and DCs; CNS inflammation in EAE is dependent on T and B cells, macrophages, and other immune cell types. Defects in any of these cell types due to *Orai3* deletion would therefore likely have been apparent in altered immune responses and disease severity. The fact that *Orai3* deletion had no effect in any of the tested disease models all but rules out a role for ORAI3 in immune function.

Deletion of *Orai3* alone may not affect SOCE in immune cells because it is compensated for by its paralogs ORAI1 and ORAI2. A similar redundancy is found in immune cells of *Orai1*-deficient mice. T cells and neutrophils of *Orai1⁻/⁻* mice have reduced (but not abolished) SOCE, CRAC currents, and effector functions (Vaeth et al., 2017b; Grimes et al., 2020). Only combined deletion

of *Orai1* and *Orai2* abolishes SOCE in T cells and neutrophils, resulting in profound functional defects in vitro and in vivo. A similar synergistic role of ORAI3 in immune cell function may be revealed in the future by the combined deletion of *Orai3* together with *Orai1* or *Orai2*. Another explanation for the normal SOCE and immune function in *Orai3⁻/⁻* mice, at least in vitro, is that our experiments have focused largely on the involvement of ORAI3 in SOCE triggered by the activation of immune receptors such as TCR, BCR, and FcR. These receptors induce SOCE via the activation of PLCγ, production of IP_3, and Ca^{2+} release from the ER, which activates STIM molecules and ORAI channels. Like its paralogs, ORAI3 forms store-operated CRAC channels because it can be activated by the depletion of ER Ca^{2+} stores, and overexpression of ORAI3 together with STIM1 generates large Ca^{2+} currents whose biophysical properties are similar to those of endogenous CRAC channels (Emrich et al., 2021). ORAI3 has been reported, however, to form another Ca^{2+} selective channel that is not activated by store depletion despite having biophysical properties similar to the CRAC channel (Lis et al., 2007). Instead, this channel is activated by low extracellular concentrations of AA (and is therefore called ARC channel; Zhang et al., 2018). Besides their activation mechanisms, other differences between CRAC and ARC channels include their sensitivity to 2-APB and their pH dependence. In vascular smooth muscle cells (VSMCs), a similar AA-activated current was reported that is induced even more robustly by the AA metabolite leukotriene C4 (LTC_4; Zhang et al., 2013). Work by the Shuttleworth and Trebak laboratories has shown that both ORAI1 and ORAI3 are required for the activation of the ARC channel and the LTC_4-regulated Ca^{2+} (LRC) channel (Mignen et al., 2008; Zhang et al., 2014). Although store-independent ARC and LRC channels have been reported in HEK293 and VSMCs, their physiological roles in these cells has remained elusive.

It is possible that AA-mediated activation of ORAI3-containing ARC or LRC channels is involved in immune cell function. Evidence in support of such a role comes from a recent study reporting that ORAI3 is upregulated in $CD4^+$ T cells from patients with RA and psoriatic arthritis (Ye et al., 2021). T cells of RA patients had increased AA-induced Ca^{2+} influx compared with those from healthy controls, and AA-induced Ca^{2+} influx in naive $CD4^+$ T cells from healthy donors could be suppressed by siRNA-mediated knockdown of ORAI3. Moreover, siRNA-mediated knockdown of ORAI3 in peripheral blood mononuclear cells of RA patients attenuated inflammation in a humanized synovitis mouse model (Ye et al., 2021). An earlier study had reported that systemic silencing of *Orai3* expression by RNAi reduces the severity of CIA, which was associated with decreased

Ca^{2+} influx in splenocytes and synovial cells, proinflammatory cytokine production, collagen-specific antibodies, and osteoclast activity (Liu et al., 2015). Both studies suggest that suppression of ORAI3 function may be beneficial in the treatment of RA. By contrast, we did not observe AA-induced Ca^{2+} influx in BMDMs from WT mice. Neither were $Orai3^{-/-}$ mice protected from CIA, because macroscopic joint swelling, histological signs of joint inflammation and destruction, proinflammatory cytokine production, and levels of anti-collagen antibodies were comparable in $Orai3$-deficient and WT mice. The discrepancies between our study and those cited above may have several reasons. Protection from synovitis in the human synovium chimeric mouse model (Ye et al., 2021) and joint inflammation and erosion in the murine CIA model (Liu et al., 2015) were observed following acute deletion of ORAI3 expression by RNAi. By contrast, constitutive germline deletion of $Orai3$ in knockout mice in our study failed to attenuate CIA severity. It is possible that lack of ORAI3 during immune cell development in $Orai3^{-/-}$ mice is compensated for by other Ca^{2+} channels. It is unlikely that these channels are ORAI1 or ORAI2, because their expression was not altered in macrophages and B cells of $Orai3^{-/-}$ mice.

It is interesting to think of ORAI3 as a Ca^{2+} influx channel in the context of inflammation. AA and its metabolites are involved in many inflammatory disease processes including RA, type 1 diabetes mellitus, and allergic asthma (Wang et al., 2021). One such metabolite is LTC_4, and cytosolic LTC_4 was shown to activate the Ca^{2+}-selective LRC channel in VSMCs. The function of the LRC channel depends on ORAI1, ORAI3, and STIM1, but not on ER Ca^{2+} store depletion (Gonzalez-Cobos et al., 2013). It is tempting to speculate that some of the roles of LTC_4 in inflammatory diseases such as allergic asthma are mediated by the induction of Ca^{2+} signals through ORAI3, but evidence for such a role is currently lacking.

Another intriguing aspect of Ca^{2+} signaling through ORAI3 channels in the context of inflammation is the fact that Ca^{2+} influx through ORAI3 is not suppressed by H_2O_2. ORAI3 is resistant to suppression of its Ca^{2+} channel function by H_2O_2 because, unlike ORAI1, it lacks a reactive cysteine in its second extracellular loop, whose thiol oxidation impairs CRAC channel function (Bogeski et al., 2010). Neutrophils and macrophages are recruited to sites of inflammation and produce large quantities of ROS, which serves as a host defense mechanism against invading pathogens but is detrimental in the context of autoimmune diseases. ORAI3 expression is upregulated relative to ORAI1 in activated human T cells, which might render T cells resistant to inhibition of Ca^{2+} influx and T cell function in inflamed tissues with high levels of ROS. It is tempting to speculate that the absence of ORAI3 in $Orai3^{-/-}$ mice results in CRAC channels that are formed predominantly by ORAI1 and susceptible to ROS-mediated inhibition. This mechanism might contribute to the attenuation of synovitis and CIA in the studies cited above in which ORAI3 expression was silenced by RNAi (Liu et al., 2015; Ye et al., 2021). Indeed, increased ROS formation and oxidative stress were reported to be associated with disease activity in RA (Mateen et al., 2016). Besides RA, oxidative stress may play major roles in the pathogenesis of MS, not only by causing demyelination and axonal damage, but also by

regulating the function of T cells and macrophages in the CNS (Ohl et al., 2016). We had therefore expected that deletion of ORAI3 would result in attenuated inflammation in the joints and CNS of $Orai3^{-/-}$ mice following induction of CIA and EAE, respectively. However, this was not the case, as $Orai3^{-/-}$ mice were as susceptible to the induction of CIA and EAE as WT mice. Moreover, SOCE in $CD4^+$ T cells isolated from the joint-draining lymph nodes of $Orai3^{-/-}$ mice with CIA was comparable to that in T cells from WT mice. ROS levels are also increased in the tumor microenvironment due to ROS production by cancer cells themselves and cells infiltrating the tumors (Weinberg et al., 2019). Tumor-infiltrating T cells therefore are exposed to high concentrations of ROS, which we hypothesized would result in reduced SOCE, impaired cytotoxic T cell function, and enhanced tumor growth. Deletion of $Orai3$, however, had no effect on $CD8^+$ T cell–mediated antitumor immunity. Together, our findings are unable to support a model in which deletion of ORAI3 results in relatively increased ORAI1 presence in the CRAC channel pore complex and enhanced susceptibility to ROS-mediated suppression of SOCE and immune responses in vivo.

Our study demonstrates that ORAI3 is dispensable for the function of T cells, B cells, and macrophages and for the regulation of immune responses in vivo. It is noteworthy that ORAI3 is upregulated in several types of cancer including estrogen receptor–positive breast cancer as well as prostate, lung, and colorectal cancer (Tanwar et al., 2020). Increased $Orai3$ expression was shown to correlate with enhanced SOCE and ARC channel activity and increased tumor cell invasion and proliferation (Tanwar et al., 2020; Sanchez-Collado et al., 2021). Moreover, deletion of ORAI3 using genetic approaches impaired tumor invasion and proliferation but enhanced tumor cell apoptosis. In light of these reports and our findings in this study, inhibition of ORAI3 channel function can see be seen as a potentially useful approach to suppress tumor growth and invasiveness without compromising immune function.

Acknowledgments

bioinformatic analyses; L. Wang, L. Noyer, Y.-H. Wang, A.Y. Tao, W. Li, J. Zu, P. Saavedra, J. Yang, and S. Feske analyzed data and interpreted the results; L. Wang and S. Feske wrote the manuscript.

References

Amarante-Mendes, G.P., S. Adjemian, L.M. Branco, L.C. Zanetti, R. Weinlich, and K.R. Bortoluci. 2018. Pattern recognition receptors and the host cell death molecular machinery. *Front. Immunol.* 9:2379. https://doi.org/10.3389/fimmu.2018.02379

Bakowski, D., F. Murray, and A.B. Parekh. 2021. Store-operated Ca²⁺ channels: Mechanism, function, pharmacology, and therapeutic targets. *Annu. Review Pharmacol. Toxicol.* 61:629–654. https://doi.org/10.1146/annurev-pharmtox-031620-105135

Benzerdjeb, N., H. Sevestre, A. Ahidouch, and H. Ouadid-Ahidouch. 2016. Orai3 is a predictive marker of metastasis and survival in resectable lung adenocarcinoma. *Oncotarget*. 7:81588–81597. https://doi.org/10.18632/oncotarget.13149

Berry, C.T., X. Liu, A. Myles, S. Nandi, Y.H. Chen, U. Hershberg, I.E. Brodsky, M.P. Cancro, C.J. Lengner, M.J. May, et al. 2020. BCR-induced Ca²⁺ signals dynamically tune survival, metabolic reprogramming, and proliferation of naive B cells. *Cell Rep.* 31:107474. https://doi.org/10.1016/j.celrep.2020.03.038

Bogeski, I., C. Kummerow, D. Al-Ansary, E.C. Schwarz, R. Koehler, D. Kozai, N. Takahashi, C. Peinelt, D. Griesemer, M. Bozem, et al. 2010. Differential redox regulation of ORAI ion channels: A mechanism to tune cellular calcium signaling. *Sci. Signal.* 3:ra24. https://doi.org/10.1126/scisignal.2000672

Cai, X. 2007. Molecular evolution and functional divergence of the Ca²⁺ sensor protein in store-operated Ca²⁺ entry: Stromal interaction molecule. *PLoS One*. 2. e609. https://doi.org/10.1371/journal.pone.0000609

Caravagna, C., A. Jaouen, S. Desplat-Jego, K.K. Fenrich, E. Bergot, H. Luche, P. Grenot, G. Rougon, M. Malissen, and F. Debarbieux. 2018. Diversity of innate immune cell subsets across spatial and temporal scales in an EAE mouse model. *Sci. Rep.* 8:5146. https://doi.org/10.1038/s41598-018-22872-y

Chan, Y.K., and M.U. Gack. 2016. Viral evasion of intracellular DNA and RNA sensing. *Nat. Rev. Microbiol.* 14:360–373. https://doi.org/10.1038/nrmicro.2016.45

Chari, R., P. Mali, M. Moosburner, and G.M. Church. 2015. Unraveling CRISPR-Cas9 genome engineering parameters via a library-on-library approach. *Nat. Methods*. 12:823–826. https://doi.org/10.1038/nmeth.3473

Chen-Engerer, H.J., J. Hartmann, R.M. Karl, J. Yang, S. Feske, and A. Konnerth. 2019. Two types of functionally distinct Ca²⁺ stores in hippocampal neurons. *Nat. Commun.* 10:3223. https://doi.org/10.1038/s41467-019-11207-8

Cheng, Y., T.N. Marion, X. Cao, W. Wang, and Y. Cao. 2018. Park7: A novel therapeutic target for macrophages in sepsis-induced immunosuppression. *Front. Immunol.* 9:2632. https://doi.org/10.3389/fimmu.2018.02632

Chu, F., M. Shi, C. Zheng, D. Shen, J. Zhu, X. Zheng, and L. Cui. 2018. The roles of macrophages and microglia in multiple sclerosis and experimental autoimmune encephalomyelitis. *J. Neuroimmunol.* 318:1–7. https://doi.org/10.1016/j.jneuroim.2018.02.015

de Graaf, C.A., J. Choi, T.M. Baldwin, J.E. Bolden, K.A. Fairfax, A.J. Robinson, C. Biben, C. Morgan, K. Ramsay, A.P. Ng, et al. 2016. Haemopedia: An expression atlas of murine hematopoietic cells. *Stem Cell Rep.*. 7:571–582. https://doi.org/10.1016/j.stemcr.2016.07.007

DeHaven, W.I., J.T. Smyth, R.R. Boyles, and J.W. Putney Jr. 2007. Calcium inhibition and calcium potentiation of Orai1, Orai2, and Orai3 calcium release-activated calcium channels. *J. Biol. Chem.* 282:17548–17556. https://doi.org/10.1074/jbc.M611374200

Emrich, S.M., R.E. Yoast, and M. Trebak. 2022. Physiological functions of CRAC channels. *Annu. Rev. Physiol.* 84:355–379. https://doi.org/10.1146/annurev-physiol-052521-013426

Feske, S. 2010. CRAC channelopathies. *Pflugers Arch.* 460:417–435. https://doi.org/10.1007/s00424-009-0777-5

Feske, S. 2019. CRAC channels and disease: From human CRAC channelopathies and animal models to novel drugs. *Cell Calcium*. 80:112–116. https://doi.org/10.1016/j.ceca.2019.03.004

Feske, S., Y. Gwack, M. Prakriya, S. Srikanth, S.H. Puppel, B. Tanasa, P.G. Hogan, R.S. Lewis, M. Daly, and A. Rao. 2006. A mutation in Orai1 causes immune deficiency by abrogating CRAC channel function. *Nature*. 441:179–185. https://doi.org/10.1038/nature04702

Fukushima, M., T. Tomita, A. Janoshazi, and J.W. Putney. 2012. Alternative translation initiation gives rise to two isoforms of Orai1 with distinct plasma membrane mobilities. *J. Cell Sci.* 125:4354–4361. https://doi.org/10.1242/jcs.104919

Gammons, J., M. Trebak, and S. Mancarella. 2021. Cardiac-specific deletion of Orai3 leads to severe dilated cardiomyopathy and heart failure in mice. *J. Am. Heart Assoc.* 10:e019486. https://doi.org/10.1161/JAHA.120.019486

Gonzalez-Cobos, J.C., X. Zhang, W. Zhang, B. Ruhle, R.K. Motiani, R. Schindl, M. Muik, A.M. Spinelli, J.M. Bisaillon, A.V. Shinde, et al. 2013. Store-independent Orai1/3 channels activated by intracrine leukotriene C4: Role in neointimal hyperplasia. *Circ. Res.* 112:1013–1025. https://doi.org/10.1161/CIRCRESAHA.111.300220

Grimes, D., R. Johnson, M. Pashos, C. Cummings, C. Kang, G.R. Sampedro, E. Tycksen, H.J. McBride, R. Sah, C.A. Lowell, and R.A. Clemens. 2020. ORAI1 and ORAI2 modulate murine neutrophil calcium signaling, cellular activation, and host defense. *Proc. Natl. Acad. Sci. USA.* 117:24403–24414. https://doi.org/10.1073/pnas.2008032117

Guiducci, C., G. Ott, J.H. Chan, E. Damon, C. Calacsan, T. Matray, K.D. Lee, R.L. Coffman, and F.J. Barrat. 2006. Properties regulating the nature of the plasmacytoid dendritic cell response to Toll-like receptor 9 activation. *J. Exp. Med.* 203:1999–2008. https://doi.org/10.1084/jem.20060401

Heng, T.S.P., and M.W. Painter, and Immunological Genome Project Consortium. 2008. The immunological genome project: Networks of gene expression in immune cells. *Nat. Immunol.* 9:1091–1094. https://doi.org/10.1038/ni1008-1091

Hoth, M., and B.A. Niemeyer. 2013. The neglected CRAC proteins: Orai2, Orai3, and STIM2. *Curr. Top. Membr.* 71:237–271. https://doi.org/10.1016/B978-0-12-407870-3.00010-X

Ibrahim, S., H. Dakik, C. Vandier, R. Chautard, G. Paintaud, F. Mazurier, T. Lecomte, M. Gueguinou, and W. Raoul. 2019. Expression profiling of calcium channels and calcium-activated potassium channels in colorectal cancer. *Cancers*. 11:561. https://doi.org/10.3390/cancers11040561

Inglis, J.J., E. Simelyte, F.E. McCann, G. Criado, and R.O. Williams. 2008. Protocol for the induction of arthritis in C57BL/6 mice. *Nat. Protoc.* 3:612–618. https://doi.org/10.1038/nprot.2008.19

Kaschek, L., S. Zophel, A. Knorck, and M. Hoth. 2021. A calcium optimum for cytotoxic T lymphocyte and natural killer cell cytotoxicity. *Semin. Cell Dev. Biol.* 115:10–18. https://doi.org/10.1016/j.semcdb.2020.12.002

Kaufmann, U., P.J. Shaw, L. Kozhaya, R. Subramanian, K. Gaida, D. Unutmaz, H.J. McBride, and S. Feske. 2016. Selective ORAI1 inhibition ameliorates autoimmune central nervous system inflammation by suppressing effector but not regulatory T cell function. *J. Immunol.* 196:573–585. https://doi.org/10.4049/jimmunol.1501406

Kayagaki, N., I.B. Stowe, B.L. Lee, K. O'Rourke, K. Anderson, S. Warming, T. Cuellar, B. Haley, M. Roose-Girma, Q.T. Phung, et al. 2015. Caspase-11 cleaves gasdermin D for non-canonical inflammasome signalling. *Nature*. 526:666–671. https://doi.org/10.1038/nature15541

Lacruz, R.S., and S. Feske. 2015. Diseases caused by mutations in ORAI1 and STIM1. *Ann. N. Y. Acad. Sci.* 1356:45–79. https://doi.org/10.1111/nyas.12938

Li, D., and M. Wu. 2021. Pattern recognition receptors in health and diseases. *Signal Transduct. Target. Ther.* 6:291. https://doi.org/10.1038/s41392-021-00687-0

Lilley, E., R. Armstrong, N. Clark, P. Gray, P. Hawkins, K. Mason, N. Lopez-Salesansky, A.K. Stark, S.K. Jackson, C. Thiemermann, and M. Nandi. 2015. Refinement of animal models of sepsis and septic shock. *Shock*. 43:304–316. https://doi.org/10.1097/SHK.0000000000000318

Lis, A., C. Peinelt, A. Beck, S. Parvez, M. Monteilh-Zoller, A. Fleig, and R. Penner. 2007. CRACM1, CRACM2, and CRACM3 are store-operated Ca²⁺ channels with distinct functional properties. *Curr. Biol.* 17:794–800. https://doi.org/10.1016/j.cub.2007.03.065

Liu, S., T. Kiyoi, E. Takemasa, and K. Maeyama. 2015. Systemic lentivirus-mediated delivery of short hairpin RNA targeting calcium release-activated calcium channel 3 as gene therapy for collagen-induced arthritis. *J. Immunol.* 194:76–83. https://doi.org/10.4049/jimmunol.1401976

Luan, S., and C. Wang. 2021. Calcium signaling mechanisms across kingdoms. *Annu. Rev. Cell Dev. Biol.* 37:311–340. https://doi.org/10.1146/annurev-cellbio-120219-035210

Ma, J., C.A. McCarl, S. Khalil, K. Luthy, and S. Feske. 2010. T-cell-specific deletion of STIM1 and STIM2 protects mice from EAE by impairing the effector functions of Th1 and Th17 cells. *Eur. J. Immunol.* 40:3028–3042. https://doi.org/10.1002/eji.201040614

Man, S.M., R. Karki, and T.D. Kanneganti. 2017. Molecular mechanisms and functions of pyroptosis, inflammatory caspases and inflammasomes in infectious diseases. *Immunol. Rev.* 277:61–75. https://doi.org/10.1111/imr.12534

Mateen, S., S. Moin, A.Q. Khan, A. Zafar, and N. Fatima. 2016. Increased reactive oxygen species formation and oxidative stress in rheumatoid arthritis. *PLoS One.* 11:e0152925. https://doi.org/10.1371/journal.pone.0152925

Matsumoto, M., Y. Fujii, A. Baba, M. Hikida, T. Kurosaki, and Y. Baba. 2011. The calcium sensors STIM1 and STIM2 control B cell regulatory function through interleukin-10 production. *Immunity.* 34:703–714. https://doi.org/10.1016/j.immuni.2011.03.016

McCarl, C.A., S. Khalil, J. Ma, M. Oh-hora, M. Yamashita, J. Roether, T. Kawasaki, A. Jairaman, Y. Sasaki, M. Prakriya, and S. Feske. 2010. Store-operated Ca^{2+} entry through ORAI1 is critical for T cell-mediated autoimmunity and allograft rejection. *J. Immunol.* 185:5845–5858. https://doi.org/10.4049/jimmunol.1001796

Mignen, O., J.L. Thompson, and T.J. Shuttleworth. 2008. Both Orai1 and Orai3 are essential components of the arachidonate-regulated Ca^{2+}-selective (ARC) channels. *J. Physiol.* 586:185–195. https://doi.org/10.1113/jphysiol.2007.146258

Morita, S., T. Kojima, and T. Kitamura. 2000. Plat-E: An efficient and stable system for transient packaging of retroviruses. *Gene Ther.* 7:1063–1066. https://doi.org/10.1038/sj.gt.3301206

Ng, C., M. Aichinger, T. Nguyen, C. Au, T. Najar, L. Wu, K.R. Mesa, W. Liao, J.P. Quivy, B. Hubert, et al. 2019. The histone chaperone CAF-1 cooperates with the DNA methyltransferases to maintain Cd4 silencing in cytotoxic T cells. *Genes Dev.* 33:669–683. https://doi.org/10.1101/gad.322024.118

Ohl, K., K. Tenbrock, and M. Kipp. 2016. Oxidative stress in multiple sclerosis: Central and peripheral mode of action. *Exp. Neurol.* 277:58–67. https://doi.org/10.1016/j.expneurol.2015.11.010

Peinelt, C., A. Lis, A. Beck, A. Fleig, and R. Penner. 2008. 2-Aminoethoxydiphenyl borate directly facilitates and indirectly inhibits STIM1-dependent gating of CRAC channels. *J. Physiol.* 586: 3061–3073. https://doi.org/10.1113/jphysiol.2008.151365

Perales-Linares, R., and S. Navas-Martin. 2013. Toll-like receptor 3 in viral pathogenesis: Friend or foe? *Immunology.* 140:153–167. https://doi.org/10.1111/imm.12143

Pierson, E.R., C.A. Wagner, and J.M. Goverman. 2018. The contribution of neutrophils to CNS autoimmunity. *Clin. Immunol.* 189:23–28. https://doi.org/10.1016/j.clim.2016.06.017

Prakriya, M., and R.S. Lewis. 2015. Store-operated calcium channels. *Physiol. Rev.* 95:1383–1436. https://doi.org/10.1152/physrev.00020.2014

Ran, F.A., P.D. Hsu, J. Wright, V. Agarwala, D.A. Scott, and F. Zhang. 2013. Genome engineering using the CRISPR-Cas9 system. *Nat. Protoc.* 8: 2281–2308. https://doi.org/10.1038/nprot.2013.143

Rangachari, M., and V.K. Kuchroo. 2013. Using EAE to better understand principles of immune function and autoimmune pathology. *J. Autoimmun.* 45:31–39. https://doi.org/10.1016/j.jaut.2013.06.008

Sanchez-Collado, J., I. Jardin, J.J. Lopez, V. Ronco, G.M. Salido, C. Dubois, N. Prevarskaya, and J.A. Rosado. 2021. Role of Orai3 in the pathophysiology of cancer. *Int. J. Mol. Sci.* 22:11426. https://doi.org/10.3390/ijms222111426

Schindl, R., J. Bergsmann, I. Frischauf, I. Derler, M. Fahrner, M. Muik, R. Fritsch, K. Groschner, and C. Romanin. 2008. 2-aminoethoxydiphenyl borate alters selectivity of Orai3 channels by increasing their pore size. *J. Biol. Chem.* 283:20261–20267. https://doi.org/10.1074/jbc.M803101200

Schuhmann, M.K., D. Stegner, A. Berna-Erro, S. Bittner, A. Braun, C. Kleinschnitz, G. Stoll, H. Wiendl, S.G. Meuth, and B. Nieswandt. 2010. Stromal interaction molecules 1 and 2 are key regulators of autoreactive T cell activation in murine autoimmune central nervous system inflammation. *J. Immunol.* 184:1536–1542. https://doi.org/10.4049/jimmunol.0902161

Shaw, P.J., C. Weidinger, M. Vaeth, K. Luethy, S.M. Kaech, and S. Feske. 2014. CD4$^+$ and CD8$^+$ T cell-dependent antiviral immunity requires STIM1 and STIM2. *J. Clin. Invest.* 124:4549–4563. https://doi.org/10.1172/JCI76602

Shuttleworth, T.J. 2012. Orai3--the "exceptional" Orai? *J. Physiol.* 590:241–257. https://doi.org/10.1113/jphysiol.2011.220574

Shuttleworth, T.J., J.L. Thompson, and O. Mignen. 2004. ARC channels: A novel pathway for receptor-activated calcium entry. *Physiology.* 19: 355–361. https://doi.org/10.1152/physiol.00018.2004

Stegner, D., S. Hofmann, M.K. Schuhmann, P. Kraft, A.M. Herrmann, S. Popp, M. Hohn, M. Popp, V. Klaus, A. Post, et al. 2019. Loss of Orai2-mediated capacitative Ca^{2+} entry is neuroprotective in acute ischemic stroke. *Stroke.* 50:3238–3245. https://doi.org/10.1161/STROKEAHA.119.025357

Takeuchi, O., and S. Akira. 2010. Pattern recognition receptors and inflammation. *Cell.* 140:805–820. https://doi.org/10.1016/j.cell.2010.01.022

Tang, W., Y. Lu, Q.Y. Tian, Y. Zhang, F.J. Guo, G.Y. Liu, N.M. Syed, Y. Lai, E.A. Lin, L. Kong, et al. 2011. The growth factor progranulin binds to TNF receptors and is therapeutic against inflammatory arthritis in mice. *Science.* 332:478–484. https://doi.org/10.1126/science.1199214

Tanwar, J., S. Arora, and R.K. Motiani. 2020. Orai3: Oncochannel with therapeutic potential. *Cell Calcium.* 90:102247. https://doi.org/10.1016/j.ceca.2020.102247

Trebak, M., and J.P. Kinet. 2019. Calcium signalling in T cells. *Nat. Rev.. Immunol.* 19:154–169. https://doi.org/10.1038/s41577-018-0110-7

Tsvilovskyy, V., A. Solis-Lopez, D. Schumacher, R. Medert, A. Roers, U. Kriebs, and M. Freichel. 2018. Deletion of Orai2 augments endogenous CRAC currents and degranulation in mast cells leading to enhanced anaphylaxis. *Cell Calcium.* 71:24–33. https://doi.org/10.1016/j.ceca.2017.11.004

Vaeth, M., and S. Feske. 2018. Ion channelopathies of the immune system. *Curr. Opin. Immunol.* 52:39–50. https://doi.org/10.1016/j.coi.2018.03.021

Vaeth, M., S. Kahlfuss, and S. Feske. 2020. CRAC channels and calcium signaling in T cell-mediated immunity. *Trends Immunol.* 41:878–901. https://doi.org/10.1016/j.it.2020.06.012

Vaeth, M., M. Maus, S. Klein-Hessling, E. Freinkman, J. Yang, M. Eckstein, S. Cameron, S.E. Turvey, E. Serfling, F. Berberich-Siebelt, et al. 2017a. Store-operated Ca^{2+} entry controls clonal expansion of T cells through metabolic reprogramming. *Immunity.* 47:664–679.e6. https://doi.org/10.1016/j.immuni.2017.09.003

Vaeth, M., J. Yang, M. Yamashita, I. Zee, M. Eckstein, C. Knosp, U. Kaufmann, P. Karoly Jani, R.S. Lacruz, V. Flockerzi, et al. 2017b. ORAI2 modulates store-operated calcium entry and T cell-mediated immunity. *Nat. Commun.* 8:14714. https://doi.org/10.1038/ncomms14714

Vaeth, M., I. Zee, A.R. Concepcion, M. Maus, P. Shaw, C. Portal-Celhay, A. Zahra, L. Kozhaya, C. Weidinger, J. Philips, et al. 2015. Ca^{2+} signaling but not store-operated Ca^{2+} entry is required for the function of macrophages and dendritic cells. *J. Immunol.* 195:1202–1217. https://doi.org/10.4049/jimmunol.1403013

Wang, B., L. Wu, J. Chen, L. Dong, C. Chen, Z. Wen, J. Hu, I. Fleming, and D.W. Wang. 2021. Metabolism pathways of arachidonic acids: Mechanisms and potential therapeutic targets. *Signal Transduct. Targeted Ther.* 6:94. https://doi.org/10.1038/s41392-020-00443-w

Weidinger, C., P.J. Shaw, and S. Feske. 2013. STIM1 and STIM2-mediated Ca^{2+} influx regulates antitumour immunity by CD8$^+$ T cells. *EMBO Mol. Med.* 5:1311–1321. https://doi.org/10.1002/emmm.201302989

Weinberg, F., N. Ramnath, and D. Nagrath. 2019. Reactive oxygen species in the tumor microenvironment: An overview. *Cancers.* 11:1191. https://doi.org/10.3390/cancers11081191

Ye, Z., Y. Shen, K. Jin, J. Qiu, B. Hu, R.R. Jadhav, K. Sheth, C.M. Weyand, and J.J. Goronzy. 2021. Arachidonic acid-regulated calcium signaling in T cells from patients with rheumatoid arthritis promotes synovial inflammation. *Nat. Commun.* 12:907. https://doi.org/10.1038/s41467-021-21242-z

Yu, L., and P. Liu. 2021. Cytosolic DNA sensing by cGAS: Regulation, function, and human diseases. *Signal Transduct. Targeted Ther.* 6:170. https://doi.org/10.1038/s41392-021-00554-y

Zhang, S.L., J.A. Kozak, W. Jiang, A.V. Yeromin, J. Chen, Y. Yu, A. Penna, W. Shen, V. Chi, and M.D. Cahalan. 2008. Store-dependent and -independent modes regulating Ca^{2+} release-activated Ca^{2+} channel activity of human Orai1 and Orai3. *J. Biol. Chem.* 283:17662–17671. https://doi.org/10.1074/jbc.M801536200

Zhang, X., J.C. Gonzalez-Cobos, R. Schindl, M. Muik, B. Ruhle, R.K. Motiani, J.M. Bisaillon, W. Zhang, M. Fahrner, M. Barroso, et al. 2013. Mechanisms of STIM1 activation of store-independent leukotriene C4-regulated Ca^{2+} channels. *Mol. Cell. Biol.* 33:3715–3723. https://doi.org/10.1128/MCB.00554-13

Zhang, X., M. Gueguinou, and M. Trebak. 2018. Store-independent Orai channels regulated by STIM. *In Calcium Entry Channels in Non-Excitable Cells.* J.A. Kozak, and J.W. Putney Jr., editors. Boca Raton (FL). 197–214.

Zhang, X., W. Zhang, J.C. Gonzalez-Cobos, I. Jardin, C. Romanin, K. Matrougui, and M. Trebak. 2014. Complex role of STIM1 in the activation of store-independent Orai1/3 channels. *J. Gen. Physiol.* 143:345–359. https://doi.org/10.1085/jgp.201311084
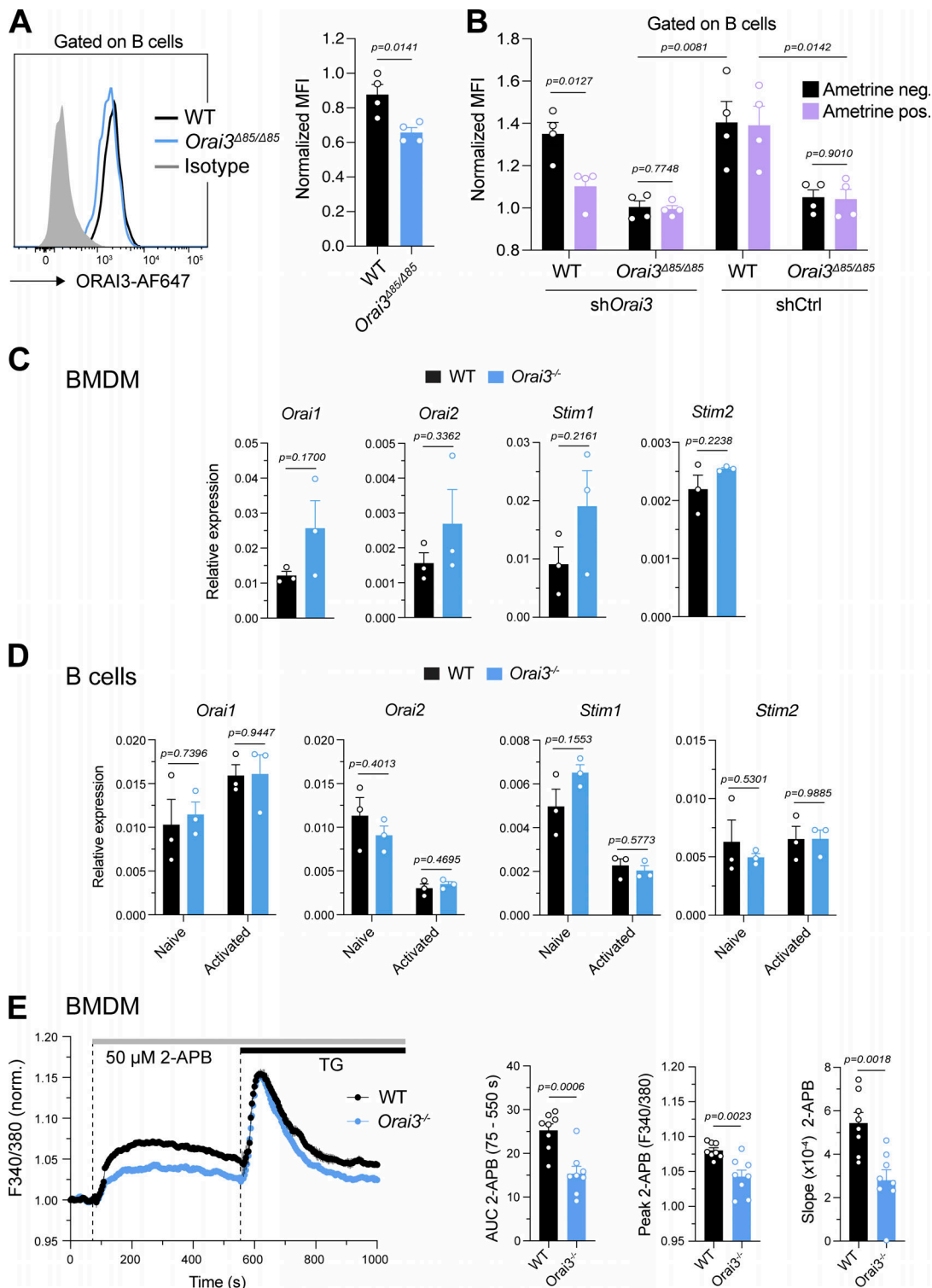
Figure S1. **Expression of *Orai3* in immune cells. (A)** Analysis of mRNA expression levels of *Orai1*, *Orai2*, and *Orai3* in hematopoietic cells using data extracted from the ImmGen database (Heng et al., 2008). Cell types were rank ordered according to relative expression of *Orai3*. Black boxes denote cell type categories. Stars next to cell type names denote B cell, macrophage, and T cell subsets. **(B)** Pearson's correlation of *Orai3* mRNA expression across different immune cell subsets using data from the ImmGen and Haemopedia (de Graaf et al., 2016) databases. Individual data points indicate TPM expression of *Orai1*, *Orai2*, or *Orai3* within a given matched cell type shared between the two datasets.

Figure S2. **Validation of *Orai3⁻/⁻* mice. (A and B)** Analysis of ORAI3 expression in B cells. **(A)** Primary murine B cells from WT and *Orai3⁻/⁻* mice were stained with isotype of anti-ORAI3 or isotype control antibody and analyzed by flow cytometry. Shown are the means ± SEM of four mice per genotype. **(B)** B cells from WT and *Orai3⁻/⁻* mice were transduced with *shRenilla* (control) and *shOrai3* plasmids encoding Ametrine. Cells were stained with anti-ORAI3 antibody and analyzed by flow cytometry. The mean fluorescence intensity (MFI) of ORAI3 expression was normalized to Ametrine-positive cells from *Orai3⁻/⁻* mice. Shown are the means ± SEM of four mice per group. **(C and D)** Relative mRNA expression of *Orai1*, *Orai2*, *Stim1*, and *Stim2* measured by qRT-PCR in WT and *Orai3⁻/⁻* BMDMs (C) and B cells left unstimulated or activated with anti-IgM/anti-CD40 for 24 h (D). Shown are means ± SEM of three mice per group. **(E)** BMDMs of WT and *Orai3⁻/⁻* mice were stimulated with 50 µM 2-APB in buffer containing 2 mM Ca²⁺, followed by stimulation with 1 µM TG. Fura-2 ratios were normalized to the average ratio in the first 20 s of recordings (baseline). Shown are representative Ca²⁺ traces from four mice per group (left) and the AUC, peak, and slope of the Ca²⁺ rise of eight mice per group as means ± SEM. Statistical analysis was performed by unpaired Student's *t* test. Exact P values are indicated in each panel.
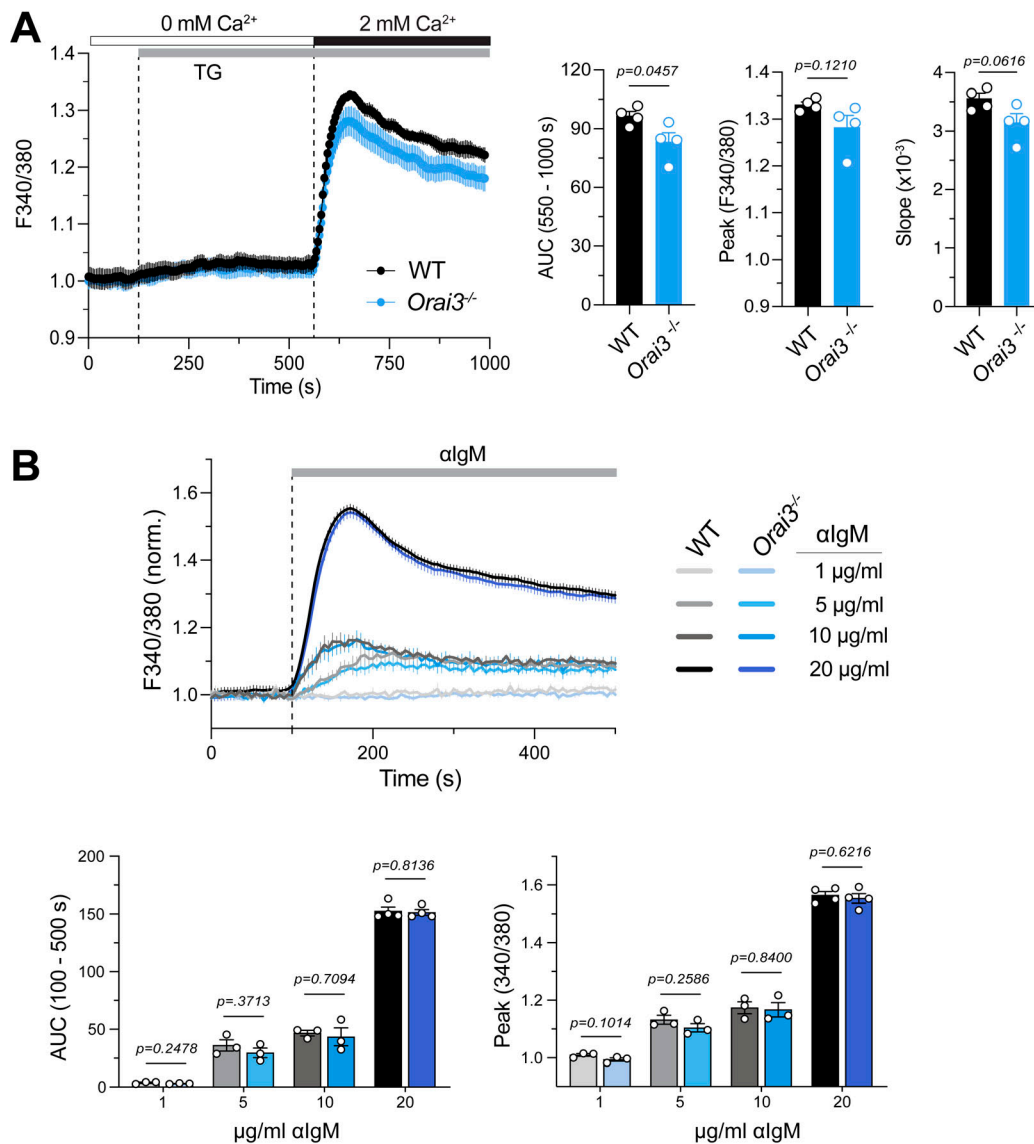
Figure S3. **B cells from *Orai3*^{−/−} mice have normal SOCE.** Analysis of SOCE in CD43⁻B220⁺ B cells isolated from the spleens of WT and *Orai3*⁻/⁻ mice and loaded with Fura-2-AM. **(A)** Ca²⁺ store depletion was induced by TG followed by induction of SOCE by readdition of 2 mM extracellular Ca²⁺. Fura-2 ratios were normalized to the average ratios in the first 20 s of the recording (baseline). SOCE was quantified as the AUC, peak, and slope of Ca²⁺ rise. Shown are Ca²⁺ traces from one representative experiment (left) and the means ± SEM of four mice and experiments per group (right). **(B)** Analysis of Ca²⁺ influx induced by BCR crosslinking with 1, 5, 10, or 20 µg/ml anti-mouse IgM antibody in Ringer's solution containing 2 mM Ca²⁺. Fura-2 ratios were normalized to the average ratios in the first 20 s. Shown are averaged Ca²⁺ traces (top) and means ± SEM of the AUC and Ca²⁺ peak from three mice per group. Statistical analysis was performed by unpaired Student's *t* test; exact P values are indicated in each panel.
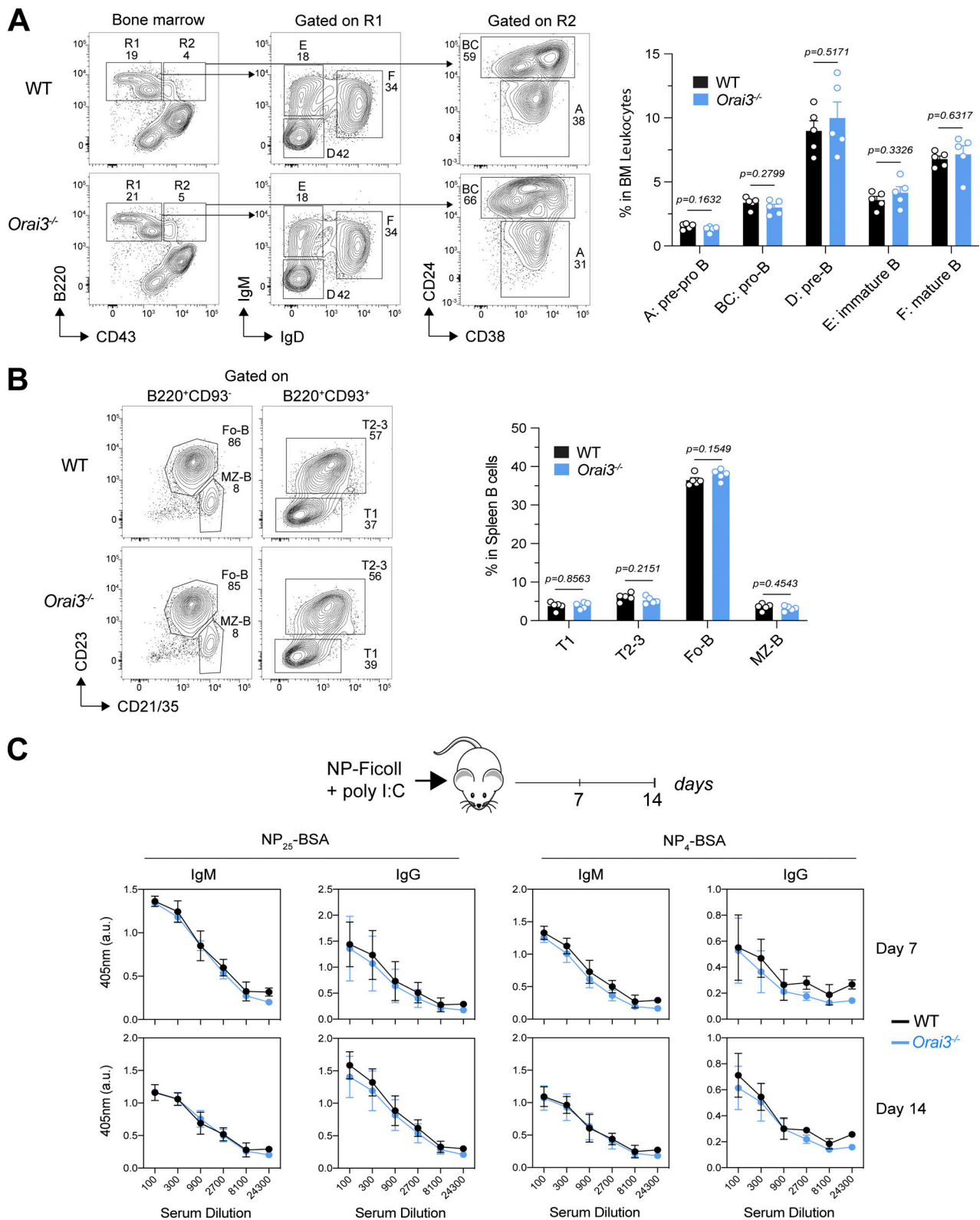
Figure S4. **Normal B cell development and function in *Orai3*−/− mice. (A)** Analysis of B cell development in bone marrow of WT and *Orai3*−/− mice. B cell subsets including pre-pro-B, pro-B, pre-B, immature B, and mature B cells were quantified by flow cytometry. Shown are mean ± SEM of five mice per genotype. **(B)** Analysis of B cell subsets in spleens from WT and *Orai3*−/− mice. Transitional B cells, follicular B cells, and marginal B cells were quantified by flow cytometry. Shown are mean ± SEM of five mice per genotype. **(C)** Analysis of the TI B cell response in WT and *Orai3*−/− mice after immunization with NP-Ficoll plus poly(I:C) in saline. Serum was collected 7 and 14 d after immunization, and ELISA was performed to detect serum antibody levels of low-affinity (binding to NP$_{25}$-BSA) and high-affinity (binding to NP$_4$-BSA) NP-specific IgM and IgG. Shown are means ± SEM of five mice per group. Statistical analysis was performed by unpaired Student's t test; exact P values are indicated in each panel.
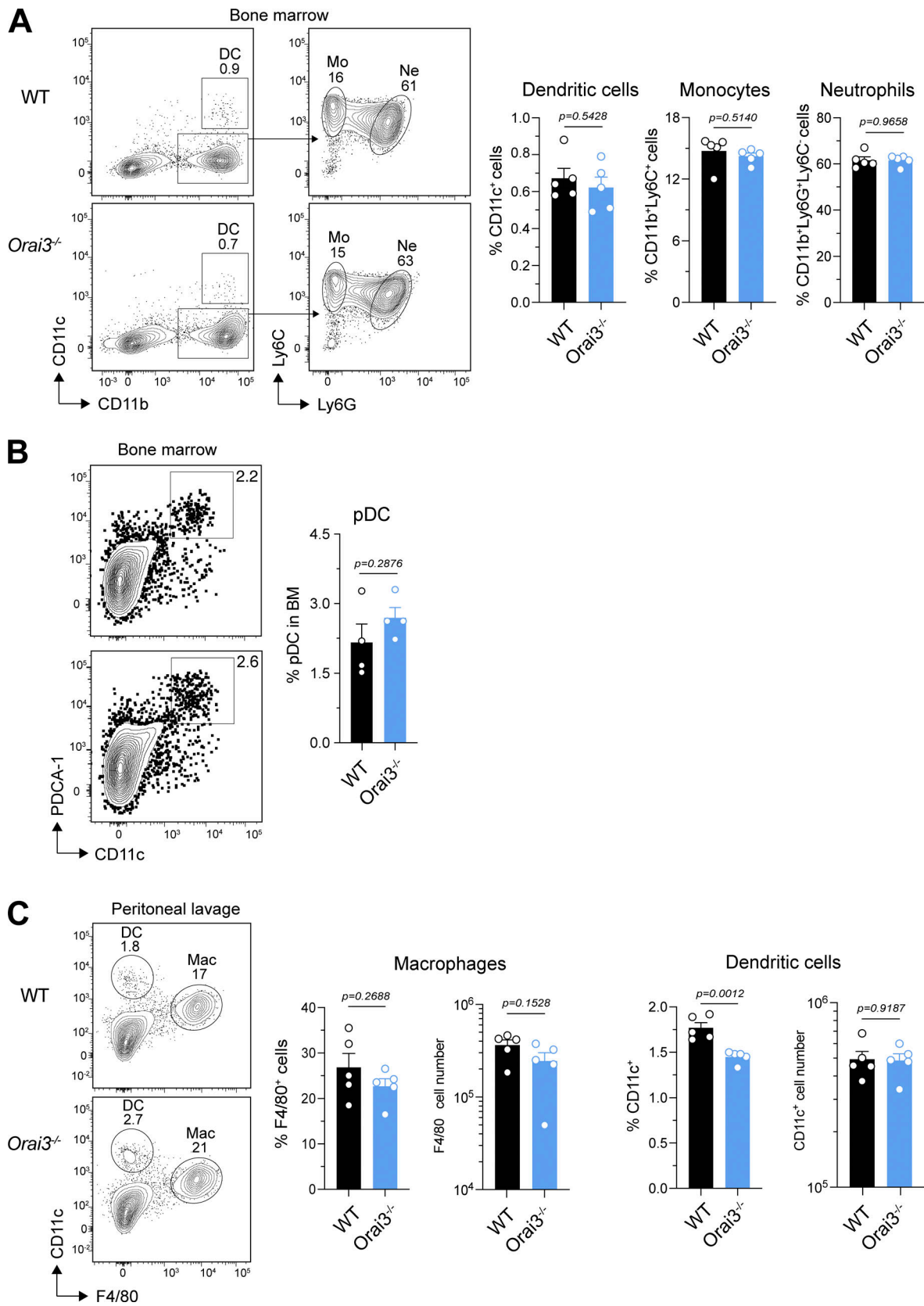
Figure S5. Normal development of myeloid cells in *Orai3*−/− mice. (A and B) Analysis of myeloid cell subsets in the bone marrow (BM) of WT and *Orai3*−/− mice. **(A)** DCs, monocytes, and neutrophils analyzed by flow cytometry. Shown are means ± SEM of five mice per group. **(B)** Frequencies of pDCs in the BM. Shown are means ± SEM of four mice per group. **(C)** Frequencies and total numbers of myeloid cells in the peritoneal cavity of WT and *Orai3*−/− mice. Shown are means ± SEM of five mice per group. Statistical analysis was performed by unpaired Student's *t* test; exact P values are indicated in each panel.

A

B

C
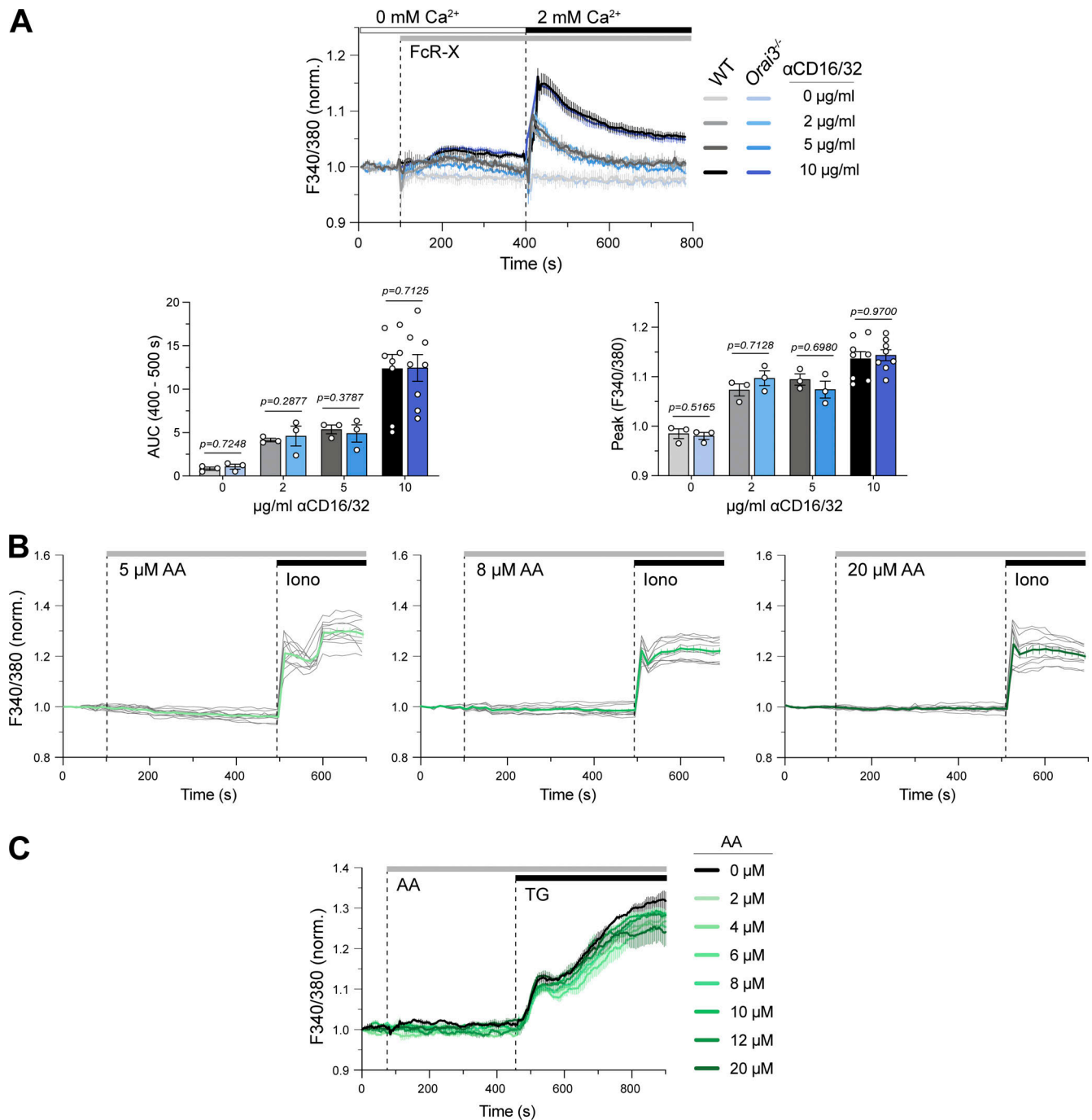
Figure S6. **Normal FcR-induced SOCE in *Orai3*-deficient macrophages.** SOCE in BMDMs. After bone marrow isolation, BMDMs were differentiated with L929 supernatant for 7 d and loaded with Fura-2-AM. **(A)** Ca^{2+} influx induced by of FcR crosslinking. BMDMs from WT and $Orai3^{-/-}$ mice were stimulated with 0, 2, 5, or 10 µg/ml anti-CD16/CD32 followed by FcR cross-linking with 30 µg/ml goat anti-rat IgG antibody in Ca^{2+}-free buffer. SOCE was induced by readdition of Ringer's solution containing 2 mM extracellular Ca^{2+}. Ca^{2+} measurements were conducted by FlexStation3 plate reader. Shown are averaged Ca^{2+} traces of three mice per group (top) and the AUC and peak Ca^{2+} of three to eight mice per group as means ± SEM. **(B)** BMDMs from WT mice were stimulated with increasing concentrations of AA in Ringer's solution containing 2 mM Ca^{2+}, followed by 1 µM ionomycin (control). Shown are representative Ca^{2+} traces of 11 cells from 1 of 3 mice (gray traces) and means ± SEM (green). Ca^{2+} measurements were conducted by fluorescence microscopy. **(C)** BMDMs were stimulated with increasing concentrations of AA in 2 mM Ca^{2+} buffer, followed by 1 µM TG as control. Ca^{2+} measurements were conducted by FlexStation3 plate reader. Shown are representative Ca^{2+} traces from one WT mouse as means ± SEM. For experiments in A–C, Fura-2 ratios were normalized to the average ratios in the first 20 s of the recording (baseline), and statistical analysis was performed by unpaired Student's *t* test; exact P values are indicated in each panel.
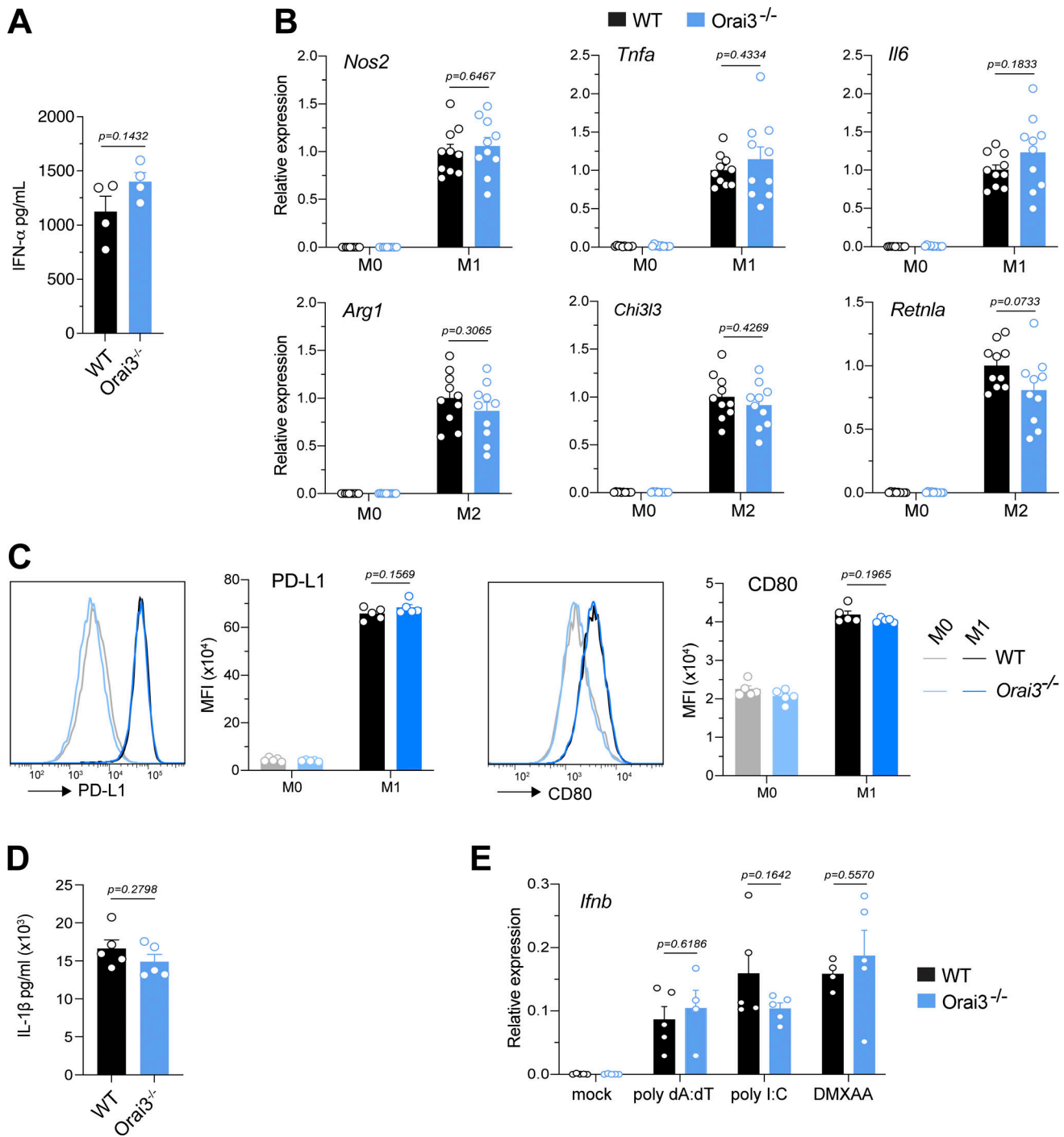
Figure S7. **Normal function of myeloid cells from *Orai3*^{−/−} mice. (A)** Total bone marrow isolated from WT and *Orai3*^{−/−} mice was stimulated with CpG-A for 24 h in vitro, and IFNα production was measured by ELISA. Shown are mean ± SEM of four mice per group. **(B and C)** Analysis of BMDM polarization into M1 and M2 macrophages. BMDMs from WT and *Orai3*^{−/−} mice were polarized into M1 or M2 macrophages with LPS + IFNγ or IL4 + IL13, respectively. **(B)** Expression of M1 markers (*Nos2, Tnfa, Il6*) and M2 markers (*Retnla, Chi3l3, Arg1*) was measured by qRT-PCR. Shown are mean ± SEM of 10 mice per group. **(C)** Expression of PD-L1 and CD80 analyzed by flow cytometry. Shown are mean ± SEM of five mice per group. **(D)** Analysis of inflammasome activation in BMDMs. BMDMs were stimulated with LPS for 4 h followed by addition of 5 µM ATP for 45 min. Levels of IL1β in the supernatant were measured by ELISA. **(E)** Analysis of IFN production by BMDMs. BMDMs were transfected with 5 µg/ml poly(dA:dT) or poly(I:C) for 6 h or stimulated with 75 µg/ml DMXAA for 2 h. IFNβ expression was measured by qRT-PCR. Shown are means ± SEM of five mice per group. Statistical analysis was performed by unpaired Student's *t* test; exact P values are indicated in each panel.
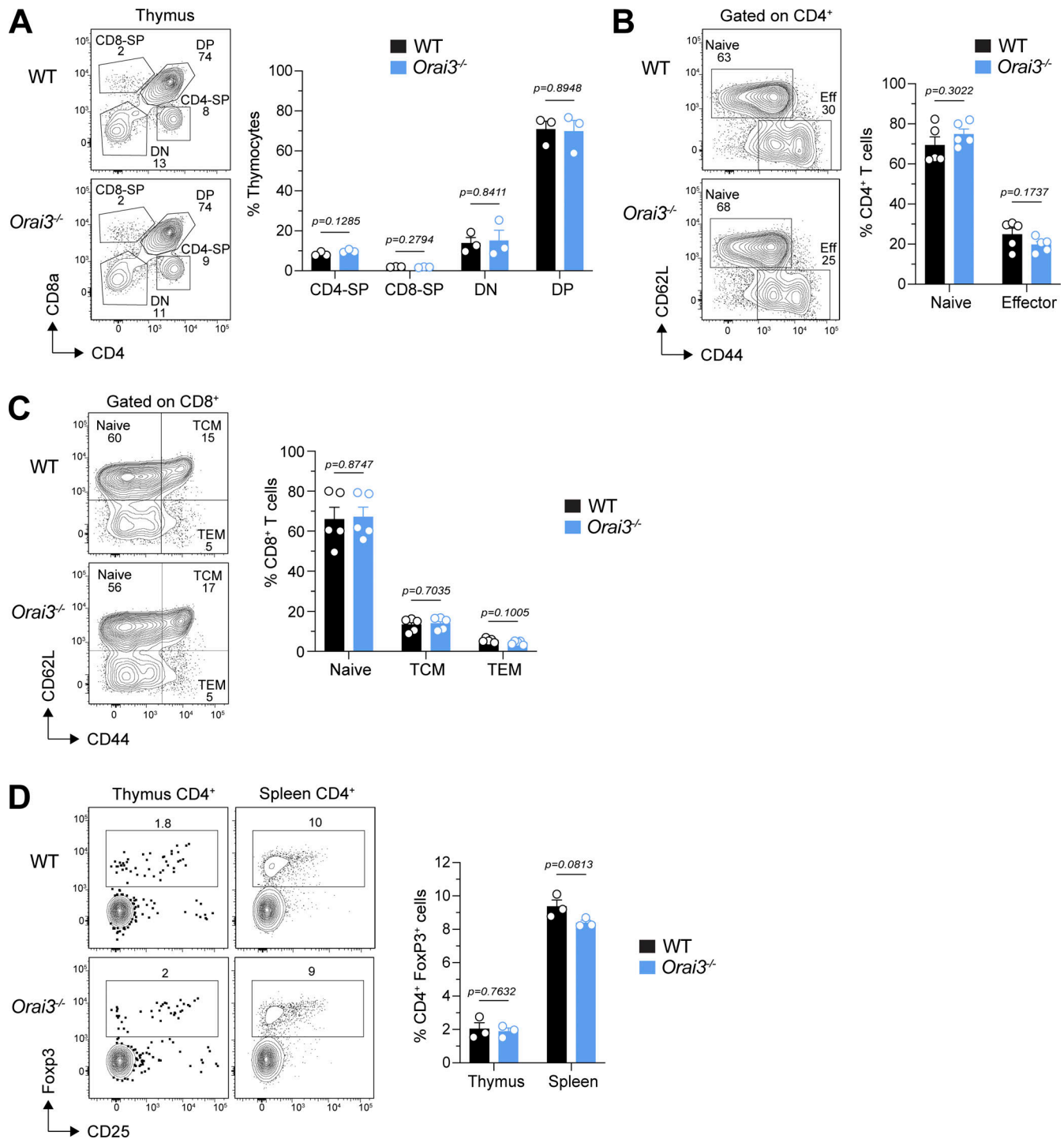
Figure S8. **Orai3$^{-/-}$ mice have normal T cell development. (A)** Analysis of thymocyte development in WT and Orai3$^{-/-}$ mice. CD4 single-positive (CD4-SP), CD8-SP, CD4 CD8 double-negative (DN), and CD4 CD8 double-positive (DP) cells were quantified by flow cytometry. Shown are representative flow cytometry plots for each genotype (left) and means ± SEM of three mice per genotype (right). **(B and C)** Analysis of naive and effector CD4$^+$ T cell and CD8$^+$ T cell frequencies in the spleen of mice. Shown are representative flow cytometry plots (left) and means ± SEM of five mice per genotype (right). **(D)** Analysis of the frequency of CD4$^+$Foxp3$^+$ Treg cells in the thymus and spleen. Shown are representative flow cytometry plots (left) and means ± SEM of three mice per genotype (right). Statistical analysis was performed by unpaired Student's t test; exact P values are indicated in each panel.
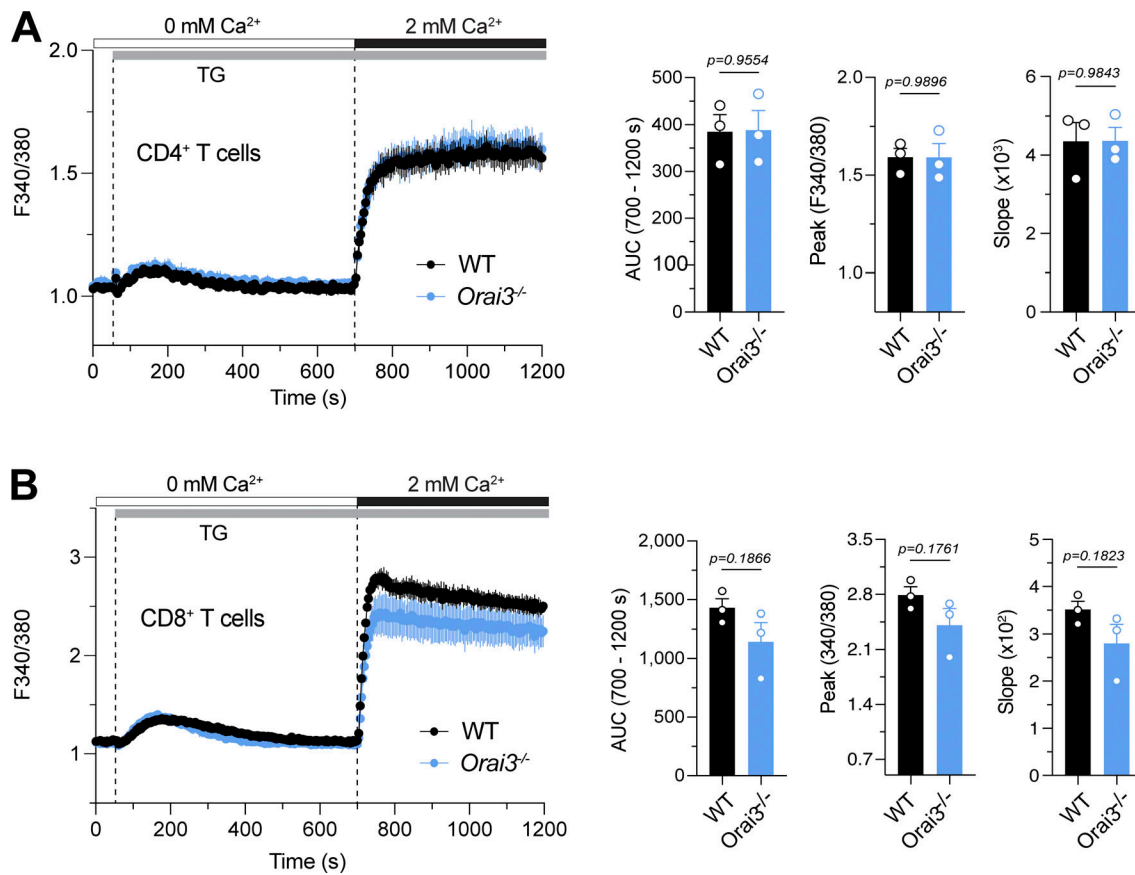
Figure S9. T cells from *Orai3⁻/⁻* mice have normal SOCE. (A and B) Analysis of SOCE in CD4+ (A) and CD8+ (B) T cells. Naive CD4+ and CD8+ T cells isolated from spleens of WT and *Orai3⁻/⁻* mice were activated with plate-bound anti-CD3/CD28 for 5 d in vitro. Cells were loaded with Fura-2-AM, and Ca^{2+} signals were measured with a FlexStation 3 plate reader. Ca^{2+} store depletion was effectuated with 1 µM TG in Ca^{2+}-free buffer, and SOCE was induced by readdition of 1 mM extracellular Ca^{2+}. SOCE was analyzed as AUC, peak, and slope of Ca^{2+} rise. Shown are Ca^{2+} traces for one representative experiment (left) and means ± SEM of three mice per genotype (right). Statistical analysis was performed by unpaired Student's *t* test; exact P values are indicated in each panel.
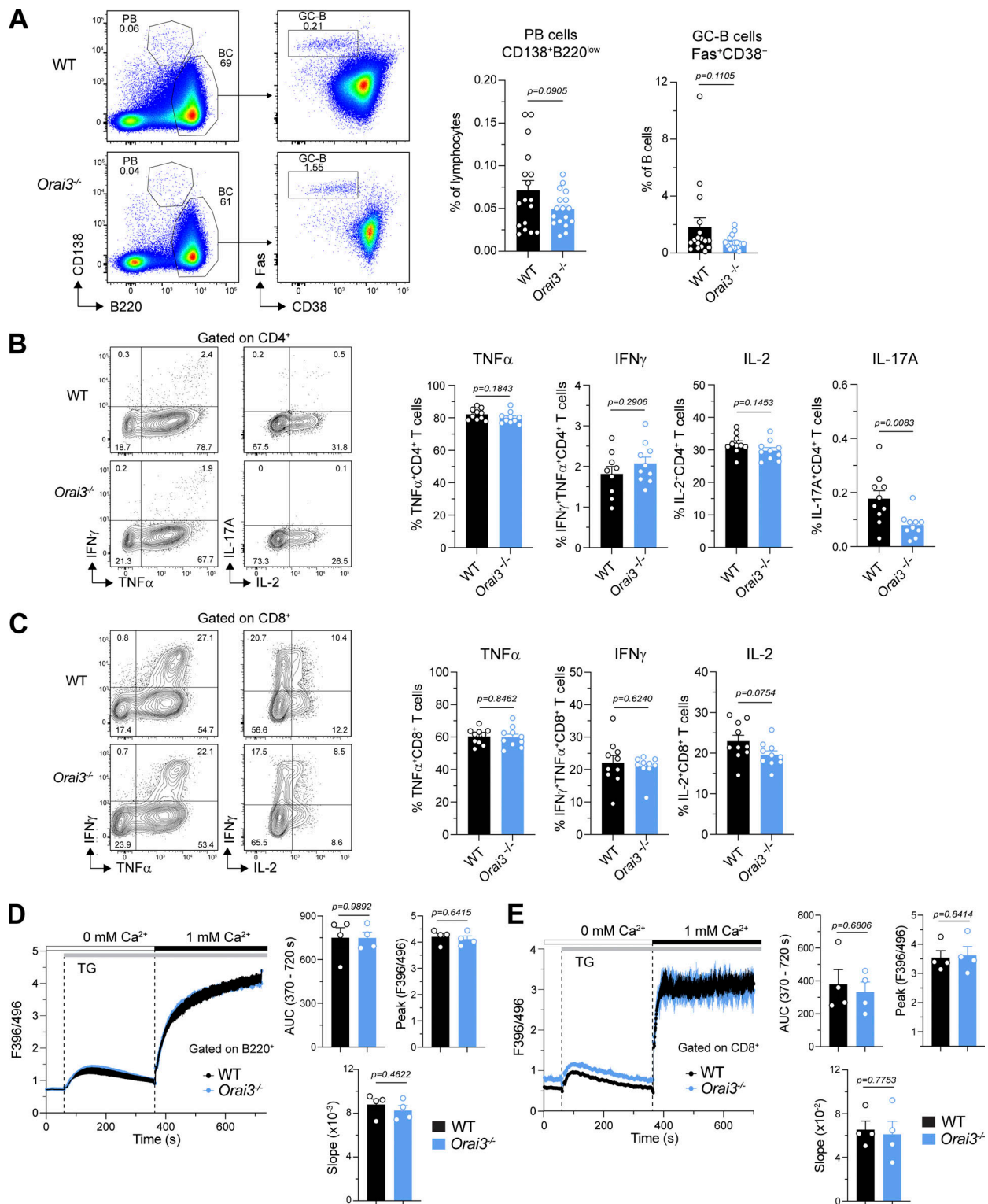
Figure S10. ***Orai3* deficiency does not protect mice from CIA. (A)** Analysis of Fas+CD38− GC B cells and CD138+ PCs in the inguinal lymph nodes (iLNs) of mice 56–59 d after induction of CIA. Shown are representative flow cytometry plots (left) and means ± SEM of 17 mice per genotype (right). **(B and C)** Analysis of cytokine production in CD4+ (B) and CD8+ (C) T cells isolated from iLNs of mice 56–59 d after induction of CIA. Intracellular levels of IFNγ, TNFα, IL-2, and IL-17A in T cells were analyzed by flow cytometry after restimulation with PMA and ionomycin for 4 h. Shown are representative flow cytometry plots (left) and mean frequencies ± SEM of 9–10 mice per genotype (right). **(D and E)** Analysis of SOCE in splenic B220+ B cells and CD8+ T cells from mice 56–59 d after induction of CIA. Cells were loaded with Indo-1 AM, and Ca2+ signals were measured by flow cytometry. Ca2+ store depletion was induced by TG in Ca2+-free buffer, and SOCE was induced by readdition of 1 mM extracellular Ca2+. SOCE was analyzed as AUC, peak, and slope of Ca2+ rise. Shown are representative Ca2+ traces (left) and means ± SEM of four mice per group (right). Statistical analysis was performed by unpaired Student's *t* test; exact P values are indicated in each panel.

Provided online are Table S1 and Table S2. Table S1 shows sgRNAs, shRNAs, genomic PCR primers, and qRT-PCR primers. Table S2 shows antibodies for flow cytometry.